T4 phage RNA is NAD-capped and alters the NAD-cap epitranscriptome of *Escherichia coli* during infection through a phage-encoded decapping enzyme

Maik Wolfram-Schauerte[1], Anastassiya Moskalchuk[1], Nadiia Pozhydaieva[1], Adán Andrés Ramírez Rojas[1], Daniel Schindler[1,2], Stefanie Kaiser[3], Nicole Pazcia[1], Katharina Höfer[1,2] *

1 Max Planck Institute for Terrestrial Microbiology, 35043 Marburg, Germany

2 SYNMIKRO, Center for Synthetic Microbiology, 35043 Marburg, Germany

3 Goethe University Frankfurt, Institute of Pharmaceutical Chemistry, 60438 Frankfurt a.M., Germany

* Corresponding author: Dr. Katharina Höfer, katharina.hoefer@synmikro.mpi-marburg.mpg.de

ABSTRACT

Nicotinamide adenine dinucleotide (NAD) serves as a cap-like structure on cellular RNAs (NAD-RNAs) in all domains of life including the bacterium *Escherichia coli*. NAD also acts as a key molecule in phage-host interactions, where bacterial immune systems deplete NAD to abort phage infection. Nevertheless, NAD-RNAs have not yet been identified during phage infections of bacteria and the mechanisms of their synthesis and degradation are unknown in this context. The T4 phage that specifically infects *E. coli* presents an important model to study phage infections, but a systematic analysis of the presence and dynamics of NAD-RNAs during T4 phage infection is lacking. Here, we investigate the presence of NAD-RNAs during T4 phage infection in a dual manner. By applying time-resolved NAD captureSeq, we identify NAD-capped host and phage transcripts and their dynamic regulation during phage infection. We provide evidence that NAD-RNAs are – as reported earlier – generated by the host RNA polymerase by initiating transcription with NAD at canonical transcription start sites. In addition, we characterize NudE.1 – a T4 phage-encoded Nudix hydrolase – as the first phage-encoded NAD-RNA decapping enzyme. T4 phages carrying inactive NudE.1 display a delayed lysis phenotype. This study investigates for the first time the dual epitranscriptome of a phage and its host, thereby introducing epitranscriptomics as an important field of phage research.

INTRODUCTION

Besides its four canonical nucleotides, RNA molecules can be decorated with diverse chemical modifications at their termini or internally (1,2). For a long time, 5′-cap-like structures on RNA were thought to exist only in eukaryotes in form of the N7-methylguanosine cap (3). However, we know today that redox cofactors, including flavin adenine dinucleotide (FAD), dephospho-coenzyme A (dpCoA) or nicotinamide adenine dinucleotide (NAD, used to refer to its oxidized form NAD^+) equip the 5′-end of RNAs as cap-like structures (4-7). NAD-capped RNAs (NAD-RNAs) are the best-studied type of these cofactor-capped RNA species regarding their identity and biosynthesis (8).

First evidence for the existence of NAD-caps *in vivo* was obtained via LC-MS analysis of total RNA (6), whilst the identity of NAD-RNAs remained unknown due to the required degradation of total RNA prior to analysis. Therefore, NAD captureSeq was developed, which allows for the chemoenzymatic capture, enrichment, and sequencing of NAD-RNAs from total RNA (5). Recently, the NAD captureSeq technology has been optimized to enhance RNA integrity and enable the sequencing of full-length NAD-RNAs. Therefore strain-promoted (copper-free) azide-alkyne cycloaddition (SPAAC) (9) and Nanopore sequencing have been applied to identify NAD-RNAs (10). Overall, based on the NAD captureSeq technology, NAD-RNAs have been identified in various bacteria (11,12), including *Escherichia coli* (5,10), archaea (13,14) and eukaryotes (9,15-21), highlighting the universal existence of this cofactor-capped RNA species (8).

The predominant – and to this day the only described – biosynthesis mechanism of NAD-RNAs involves the RNA polymerase (RNAP) that uses NAD as a non-canonical initiating nucleotide (NCIN). Instead of ATP, it incorporates NAD (with an adenosine moiety involved in base pairing) at the 5′-end of RNA *ab initio* during transcription initiation (8,22). In bacteria, the NAD-cap provides a stabilizing effect to the RNA, whilst it promotes RNA decay in eukaryotes (8). NAD-RNA decapping and subsequent degradation can occur via two pathways. DeNADding refers to the removal of the entire NAD-cap and has only been described in eukaryotes to this day (8,21,23). NAD-cap hydrolysis by Nudix hydrolases cleaves the diphosphate moiety within the NAD-cap, releasing 5′-monophosphorylated RNA, which can be subjected to cleavage afterwards (5,8,24). Apart from that the roles of NAD-RNAs are poorly understood (8).

In order to study potential roles of NAD-RNAs it may seem promising to look beyond a single organism and instead focus on, for instance, pathogen-host interactions. Such pathogen-host interactions have been studied using dual sequencing (dual-seq) approaches that simultaneously assess both the host and pathogen transcriptome (25). Dual-seq can reveal the intricate interplay of host and pathogen, but has not yet been applied to study these interactions on the level of the epitranscriptome. NAD-RNAs have only been indicated to exist during infection by the eukaryotic Dengue virus using LC-MS (7) and HIV-1 infection of human cells (26). Surprisingly, NAD is a key

regulatory molecule in the interactions between phages and their bacterial hosts. Bacteria have evolved phage defense strategies that involve the depletion of NAD to abort phage infection and phages restore NAD to counteract the defense (27-30). Despite the central role of NAD in phage infections, the dual NAD-cap epitranscriptome has not yet been studied in phage-host interactions.

As mentioned above, NAD-RNAs have been initially discovered in *E. coli* (5,31) which is – among others – infected by bacteriophage T4 (T4 phage) (32). It infects *E. coli* by injecting its 169 kb dsDNA genome and protein effectors (32). Then, a fine-tuned infection program begins to take-over the host's gene expression machinery including the RNAP and ribosomes to express phage genes (32). Therefore, the T4 phage creates the ideal environment for self-reproduction starting with host reprogramming in early, DNA replication in middle and structural phage proteins biosynthesis in late phase of infection (33,34). Moreover, the phage triggers the shut-off of host gene transcription and RNA degradation (32-34). Albeit these processes have been fundamentally understood, detailed mechanistic insights, e.g. how the RNA degradation machinery distinguishes between phage and host RNA, remains elusive. Epitranscriptomic mechanisms may provide a regulatory layer to achieve these characteristics (35). However, epitranscriptomics has only scarcely been applied to phage research. Just recently, NAD-RNAs have been found to serve as substrates for an ADP-ribosyltransferase (ART) from bacteriophage T4 (T4 phage) (36). The ART ModB uses NAD-RNAs in an RNAylation reaction, by which it covalently attaches NAD-RNAs to ribosomal proteins of its host *Escherichia coli* including ribosomal proteins S1 and L2 (36). This may provide a means for the T4 phage to regulate gene expression during infection on the translational level. Further, it indicates a distinct biological function of NAD-RNAs, namely activation of the RNA for the enzymatic transfer to a target protein (36). Apart from this role of NAD-RNAs in RNAylation of host proteins during infection, the abundance, identity, biosynthesis and degradation of NAD-RNAs during T4 phage infection are uncharacterized to this day.

Here, we study for the first time the time-resolved dual NAD-cap epitranscriptome of T4 phage infection of *E. coli*. This enables to determine the dynamic modulation of NAD-RNAs across various infection phases characterized by specific gene expression patterns. Therefore, we establish an optimized NAD captureSeq protocol including SPAAC and Nanopore sequencing allowing for accurate 5'-end determination and full-length transcript identification. Thereby, we identify the infection phase-dependent occurrence of NAD-capped T4 phage transcripts, while host NAD-RNAs decrease in abundance throughout infection. Time-resolved differential RNA-Seq suggests NAD-capping of both host and phage transcripts to occur through the host RNAP. Moreover, we present evidence for the role of the T4 phage Nudix hydrolase NudE.1 (37) in the hydrolysis of NAD and NAD-RNAs. T4 phages with catalytically inactive NudE.1 display delayed lysis indicating the important auxiliary role of this Nudix hydrolase during T4 phage infection.

Together, we here present the first study of an RNA modification in a phage-host interaction by identifying and characterizing the dynamic landscape of NAD-RNAs during T4 phage infection.

MATERIALS AND METHODS

General

All DNA and RNA oligos were purchased from Integrated DNA Technologies. Chemical compounds were obtained from Sigma Aldrich or Carl Roth GmbH, if not indicated otherwise. RNA was precipitated in the presence of 0.3 M NaOAc pH 5.5 and 1 volume isopropanol by centrifugation at 21,000 x *g* or 18,500 x *g*, 4 °C for 90 min after incubation at -20 °C overnight, if not indicated differently.

Strains, media and cultivation

Cultivation of *E. coli* strains (Supplementary Table S1) was conducted in lysogeny broth (LB) medium supplemented with the 30 µg/µL kanamycin (for pET28a-based expression strains) or without antibiotic (*E. coli* B strain) at 37 °C, 180 rpm.

Determination of E. coli cell concentration

E. coli cell concentration was determined by diluting an *E. coli* culture at an optical density at 600 nm (OD_{600}) = 0.84 1:2,000 in isotone (Sigma Aldrich) and measuring 75 µL thereof at a Coulter counter (Multisizer 4e (Beckman Coulter)). Cells counts in the range of 1 – 2 µm particle size were summed and blank background was subtracted to obtain the measure of $3 * 10^8$ *E. coli* cells per mL at OD_{600} = 0.8.

T4 phage infection

Bacteriophage T4 infection of *E. coli* strain B was performed in LB medium, supplemented with 1 mM $CaCl_2$ and 1 mM $MgCl_2$, either at room temperature (rt) shaking at 120 rpm or at 37 °C shaking at 180 rpm. OD_{600} of *E. coli* culture used for infection varied between 0.2 – 0.8 and phages were added to a final multiplicity of infection (MOI) ranging from 0.2 – 5.0.

T4 phage production

E. coli BL21 DE3 pET28a was grown to OD_{600} = 0.6 in LB medium with kanamycin at 37 °C, 180 rpm. T4 phage solution was added to a multiplicity of infection (MOI) of 0.2 and the culture incubated at room temperature, 120 rpm overnight. Unlysed cells were pelleted by centrifugation at 5,000 x *g*, 4 °C for 25 min and supernatant was filtered through 0.22 µm filters. The resulting T4 phage solution was stored in glass bottles at 4 °C.

Determination of T4 phage titer via plaque assay

T4 phage solution was diluted 10^{-1} to 10^{-11} in LB medium. 300 µL of *E. coli* B strain bacterial culture (OD_{600} = 1.0) and 100 µL of respective diluted phage solution were mixed each and incubated for 2-3 min at rt. Then, samples were mixed each with 4 mL of soft agar (2 % w/v agar, 1.5 % w/v

pepton, 0.75 % w/v yeast extract, 1.5 % w/v NaCl) preheated to 55 °C. Whole mixtures were poured onto LB agar plates and incubated at 37 °C overnight. The titer was determined using equation *1*:

$$\frac{\text{Number of plaques x dilution factor}}{\text{Volume of the phage lysate in mL}} = \frac{\text{Number of phages in pfu}}{\text{Volume of phage lysate in mL}} \qquad (1)$$

Lysis assay

E. coli B strain was grown at 37 °C, 180 rpm in LB medium supplemented with 1 mM $CaCl_2$ and 1 mM $MgCl_2$ to OD_{600} = 0.8. Then, cultures were transferred to rt shaking at 120 rpm and phage solution was added to an MOI of 1.5 – 5.0. OD_{600} was regularly monitored to determine cell lysis. Alternatively, the same assay was performed in a BioTek plate reader (Agilent) measuring cell density as OD_{600} in a 48-well format at rt shaking at 300 rpm every 3 min. For the plate reader measurement of OD_{600}, OD values were normalized to 1 at time point 0 before plotting.

Burst size assay

50 mL of *E. coli* B strain culture in LB medium supplemented with 1 mM $CaCl_2$ and 1 mM $MgCl_2$ that was grown to OD_{600} 0.8 was infected with T4 phage (WT or NudE.1 E64,65Q) at MOI 0.01 and incubated in a water bath at 37 °C. To determine the amount of all phages added, 50 µL of appropriately diluted culture at 6 minutes post infection was subjected to plaque assay as described above. At the same time point and all other subsequent time points, the culture was diluted according to the expected amount of phages (that can be assessed by plaque assay) and 1 mL free-floating phages were specifically isolated with 50 µL chloroform. 50 µL thereof were used for plaque assay as described above. The amount of initially infecting phages was calculated as the difference between all phages and free-floating phages at 6 min post infection. This was used to calculate the burst size during the first 60 min of infection.

T4 phage mutant generation and screening

Mutagenesis

E. coli BL21 DE3 containing plasmids pET28a_NgTET_NudE.1-E64,65Q and pCpf1_NudE.1 was used for mutagenesis. The cells were grown to OD_{600} = 0.4 at 37 °C, 160 rpm, when NgTET expression was induced by addition of 50 µM IPTG and cells were grown further to OD_{600} = 0.8. The cultivation was proceeded until OD_{600} of 0.8. At this point, the cultures were adjusted to room temperature shaking at 120 rpm and supplemented with 1 mM $MgCl_2$ and 1 mM $CaCl_2$. Infection was carried out with NgTET-treated T4 phage WT set to a multiplicity of infection (MOI) of 0.5 as described previously (38). The infection was performed for 3 h, at 130 rpm and 23 °C after which the cells were pelleted and supernatant filtered through 0.45 µm filters. The titer of the newly generated phages was determined via plaque assay and the phages were used for the counter-selection via infection of *E. coli* Cas13a_NudE.1 (plasmid pBA560-Cas13a-NudE.1). The counter-selection was performed under the same conditions as the mutagenesis. The counter-selected phages were

filtered through 0.45 µm filter and used for a plaque assay with *E. coli* B strain. 144 individual plaques were picked and resuspended in 200 µL Mg-Pi-buffer (26 mM Na_2PHO_4, 68 mM NaCl, 22 mM KH_2PO_4, 1 mM $MgSO_4$, pH 7.5) supplemented with 2 µL Chloroform and incubated at room temperature shaking at 500 rpm for 1 h. Plaques in solution were stored at 4 °C.

Mutant identification using long-read amplicon sequencing

Phages were screened for mutations by Nanopore sequencing as described previously (35,39). 1 µL resuspended plaque were used for each PCR in 10 µL scale in the presence of 1 x High Fidelity PCR Master Mix (NEB) and 500 nM NudE.1 fwd and rev screening primer (Supplementary Table 2) using 98 °C for 3 min followed by 30 cycles of 98 °C for 10 s, 60 °C for 10 s and 72 °C for 1 min with a final hold at 72 °C 10 min. A second dual barcoding PCR was performed using KAPA HiFi HotStart ReadyMix (Roche) in the presence of 1 µL of a 1:10 dilution of the initial PCR as template and 0.3 µM of the barcoding primers (38,39) in 7 µL reactions. PCRs were conducted at 95 °C for 3 min followed by 20 cycles of 98 °C for 20 s, 66 °C for 15 s and 72 °C for 60 s with a final extension of 72 °C for 5 min. All the barcoded PCR reactions were pooled and purified using an open source purification procedure using the NucleoMag kit for NGS library preps (Macherey Nagel) (40). Briefly, DNA was bound to magnetic beads, washed twice with 80 % ethanol and eluted in 100 µL elution buffer (5 mM Tris-HCl pH 8.5). Concentration was determined with NanoDrop (ThermoFisher Scientific) and Qubit (Invitrogen) using the broad range and/or high sensitivity assay. Sequencing libraries were generated with the SQK-LSK109 Ligation Sequencing kit (Oxford Nanopore Technologies) according to the manufacturer's guidelines starting with 1 µg of input DNA. Sequencing was performed on Flongle flow cells (R9.4.1 chemistry) on a MinION device.

Analysis of long-read sequencing data

Nanopore raw reads were basecalled using guppy (v6.4.2). Reads were analysed using the CRISPRT4 pipeline (35) (https://github.com/MaikTungsten/CRISPRT4). In a miniconda environment, reads were demultiplexed using minibar (41) and mapped to the T4 phage reference genome (NCBI: NC_000866.4, accessed 15th September 2023) using minimap2 (version 2.24) (42). The resulting SAM files were converted to BAM files, sorted, and indexed with samtools (version 1.4.1) (43). Variant calling in the target region of mutagenesis was subsequently performed using longshot (version 0.4.1) (44) and resulting VCF files were inspected for desired point mutants with Integrative Genomics Viewer (IGV 2.16.0) (45).

Recovery of T4 NudE.1 E64,65Q mutant phage

Candidate mutants were propagated by the addition of 10 µL resuspended phage plaque to 10 mL *E. coli* B strain culture in LB medium supplemented with 1 mM $MgCl_2$ and 1 mM $CaCl_2$ and incubation at room temperature, 120 rpm overnight. Sanger sequencing was performed to validate the mutation. As a small fraction of the phage population contained the WT locus of NudE.1, the phage mutant candidate was counter-selected against WT. Therefore, 10 mL *E. coli*

BL21 DE3 with plasmid pBA560-Cas13a-NudE.1 was grown in LB medium supplemented with 30 µg/mL chloramphenicol to OD_{600} = 0.4, when the expression of the Cas13a system was induced by addition of tetracycline to final concentration 1 nM. After 10 min incubation, 10 µL phage was added and incubated at 37 °C for 1 h. Thereafter, phage was purified by filtration through 0.45 µm filters, diluted in LB medium and used for plaque assay with *E. coli* BL21 DE3 with plasmid pET28-NudE.1 induced with 1 mM IPTG. Single plaques were picked again, screened with Sanger sequencing and mutant phage amplified as described above.

Total RNA isolation

100 mL LB medium with 1 mM $MgCl_2$ and 1 mM $CaCl_2$ were inoculated with overnight culture of *E. coli* strain B, *E. coli* JM109 + pUC19 (with ampicillin as an to antibiotic) OD_{600} = 0.1. The culture was incubated at 37 °C, 160 rpm to OD_{600}= 0.8. Then, the culture was transferred to rt and the first 5 mL sample was taken (0 min). Subsequently, the bacterial culture was infected with T4 phage solution to a multiplicity of infection of 1.5 or 5.0, respectively. The T4 phage-infected culture was incubated at rt, 120 rpm and 5 mL samples were taken at 1, 4, 7, 10 and 20 min of post-infection or as indicated. After sampling, cells were lysed immediately using one volume (5 mL) of the 90 °C lysis solution (2 % SDS, 4 mM EDTA) and incubated at 90 °C for 2 minutes. RNA was extracted in one volume (10 mL) of Roti-Aqua-Phenol (Carl Roth) by incubating at 67 °C for 10 min and centrifuging for 10 min and at 18,500 x *g*, rt. RNA was extracted again from the upper phase using one volume (10 mL) of Roti-Aqua-P/C/I (Carl Roth) and samples were centrifuged at 18,500 x *g*, 4 °C for 10 min. Upper phases were mixed with one volume of ice-cold isopropanol and 0.1 x volume of 3 M NaOAc pH 5.5 and incubated at -20 °C overnight. RNAs were precipitated by centrifugation at 18,500 x *g* at 4 °C for 2 h. RNA-pellets were resuspended in 450 µL RNase-free water. RNA was digested in 1 x DNaseI buffer with 0.8 U/µL of DNaseI (Roche) to remove residual DNA. Reactions were incubated at 37 °C for 40 min. DNaseI digestion was stopped by addition of one volume of Roti-Aqua-P/C/I. Samples were centrifuged at 17,000 x *g*, 1 min, rt. P/C/I-extraction was performed twice. Residual phenol was removed by diethylether extraction using one volume diethylether and phase separation by short centrifugation. The extraction was performed three times. The residual diethylether was evaporated using the SpeedVac (Thermo Fisher). RNAs were ispropanol precipitated and RNA pellets were resuspended in 20 – 100 µL RNase-free water. Final RNA concentrations were determined using the NanoDrop (Thermo Fisher). RNAs were analyzed by 10 % PAGE as well as 1 % agarose gel electrophoresis. Gels were imaged at ChemiDoc (Bio-Rad) using either SYBR Gold (Invitrogen) or PeqGreen (PreqLab) staining. Further, RNAs were analyzed using Agilent RNA 6000 Nano Kit and the Bioanalyzer system (Agilent). Thereby, RNA integrity was determined and only RNAs with RNA integrity numbers (RINs) greater than 9.0 were used for further analysis.

Preparation and characterization of NAD-RNAs by *in vitro* transcription

Amplification of Qβ and RNAI dsDNA templates

PCR of Qβ and RNAI dsDNA template for *in vitro* transcription was performed using 50 nM fwd and 50 nM rev ultramer (Supplementary Table S2) in the presence of 1 x GC buffer, 5 % DMSO, 0.1 mM of dNTP mix, 500 nM fwd primer, 500 nM rev primer and 0.01 U/µL Phusion polymerase (Thermo Fisher). The PCR products were analyzed by 2 % agarose gel electrophoresis and purified using the Qiagen PCR purification kit. DNA concentrations were measured using the NanoDrop.

IVT transcription of 5`-PPP-RNA and 5`-NAD-RNA

In vitro transcription (IVT) of 5'-triphosphate (PPP) Qβ-RNA and RNAI was performed in a 20 µL scale using the HighYield T7 RNA Synthesis Kit (Jena Bioscience) according to manufacturer's instructions in the presence of 1 µg dsDNA template. NAD-capped RNA was synthesized using the same conditions except for the presence of 3.75 mM ATP and 7.5 mM NAD. The IVT reactions were incubated at 37 °C for 3 h. Residual DNA was removed by DNase I digestion using 20 U DNase I and 1 x DNase I incubation buffer and incubating the mixture at 37 °C for 30 min. *In vitro* transcribed 5'-PPP-RNAs and 5'-NAD-RNAs were purified by 10 % preparative PAGE. RNA bands were visualized by UV shadowing. The bands were excised, and RNA was eluted from the gel material by incubation in 4 mL 0.3 M NaOAc pH 5.5 by shaking at 600 rpm, 14 °C overnight. An additional elution step was performed for 3 h at the same settings. After removal of gel pieces, RNA was isopropanol precipitated, RNA pellets were air-dried and resuspended in 200 µL RNase-free water, isopropanol-precipitated again and resuspended in a final volume of 50 µL RNase-free water. RNA concentrations were measured on the NanoDrop. NAD-RNAs were analyzed using 10 % PAGE. The presence of the NAD-cap was confirmed by 6 % APB-PAGE and NudC digest as described before (46) except for the usage of a HEPES buffered system. Reactions were prepared for analysis in a 10 µL scale by incubating 100 ng of each RNA, 1 x degradation buffer and 4.2 µM NudC (1 µL) or 1 µL RNase-free water, respectively. The reactions were incubated at 37 °C, 30 min and applied to 6 % (w.r.t. final acrylamide concentration) APB-PAGE. Gels were imaged at ChemiDoc after staining in SYBR Gold (Invitrogen).

NAD captureSeq library prep

NAD captureSeq was performed in a similar manner as described in (47).

Chemo-enzymatic labelling of total RNA

Labelling of total RNA was performed in two subsequent steps: ADPRC and SPAAC reaction. ADPRC reactions were performed in a 100 µL scale in the presence of 1 x ADPRC buffer, 10 % 3-azido-1-propanol, 70 µg total RNA from *E. coli (*before and after 1, 4, 7, 10 and 20 min of infection), 10 ng of 100 nt control NAD- RNA (spike-in, Supplementary Table S3) and in the presence or absence of 0.85 µM ADPRC. The mixtures were incubated at 37 °C for 45 min. Reactions were

stopped by Roti-Aqua-PCI extraction, followed by diethylether extraction. Then, reactions were isopropanol-precipitated in the presence of 40 µg RNA-grade glycogen. Pellets were resuspended in 20.3 µL RNase-free water.

SPAAC reactions were performed in a 40 µL scale in the presence of 20 µL RNA (~ 70 µg), 1 x PBS and 0.25 mM biotin-PEG4-DBCO (in DMSO). Reactions were incubated at 37 °C, 2 h. Then, 160 µL RNase-free water were added. Reactions were stopped by Roti-Aqua-PCI extraction, followed by diethylether extraction Samples were isopropanol-precipitated in the presence of 40 µg RNA-grade glycogen. RNA pellets were resuspended in 40.3 µL Immobilization buffer (10 mM Na-HEPES pH 7.2, 1 M NaCl, 5 mM EDTA). The integrity of RNAs after both ADPRC and SPAAC reactions was analyzed by applying of 0.3 µL (~ 1 µg) of each sample to 1 % agarose gel electrophoresis.

Preparation of streptavidin beads and capture

Mobicol classic columns (MoBiTec) were assembled with small filters and placed into 2 mL reaction tubes. 50 µL streptavidin Sepharose were added to each column. The streptavidin beads were equilibrated by washing three times with 200 µL immobilization buffer. The columns were then centrifuged at 17,000 x *g*, 1 min, rt, and the supernatants were discarded. All further wash steps mentioned were performed three times with the same volume of respective buffer with an exception for washing with streptavidin wash buffer (8 M urea, 50 mM Tris-HCl pH 7.4) and 0.25 x streptavidin wash buffer (2 M urea, 50 mM Tris-HCl pH 7.4). In these cases, the beads were washed five times. After washing, the beads were blocked by addition of 100 µL immobilization buffer, supplemented with 100 µg/mL acetylated BSA and by incubation at 20 °C, 1,000 rpm for 20 min. Then, blocking reactions were centrifuged at 17,000 x *g*, rt for 1 min and flow-through was discarded. Blocking steps were always performed in the same manner with 100 µL of respective buffer and 100 µg/mL acetylated BSA. After blocking, the streptavidin beads were washed with immobilization buffer as previously described. The biotinylated RNAs were captured by streptavidin beads by addition of their complete volume of 40 µL (~ 70 µg) to each column and incubation at 20 °C, 1,000 rpm for 1 h. The mixtures were centrifuged at 17,000 x *g*, rt for 1 min and the supernatants were discarded. Then, the beads were washed with streptavidin wash buffer.

RNA 3'-adaptor ligation

The streptavidin beads were equilibrated, blocked, and subsequently washed in the same manner as described earlier with 1 x standard ligation buffer (500 mM Tris-HCl pH 7.4, 100 mM $MgCl_2$). For the RNA 3′ adaptor ligation, the adaptor ligation mixture consisting of 5 µM adenylated 3′-adaptor, 1 x standard ligation buffer, 15 % DMSO, 50 µg/mL adenylated BSA, 50 mM 2-mercaptoethanol, 0.5 U/µL T4 RNA ligase 1 (NEB) and 10 U/µL T4 RNA ligase 2, truncated K227Q (NEB) was prepared on ice. 30 µL of this mixture were added to the beads and the columns were incubated at 4 °C overnight. Then, NaCl was added to the beads to a final concentration of 1.5 M

and the columns were incubated at 20 °C, 1,000 rpm for 1 h. After incubation, reactions were centrifuged at 17,000 x *g*, rt for 1 min. The supernatants were discarded, and the beads were washed with streptavidin wash buffer.

Reverse transcription

The streptavidin beads were equilibrated, blocked, and subsequently washed in the same manner as described with 1 x first-strand buffer (250 mM Tris-HCl pH 8.3, 375 mM KCl, 15 mM $MgCl_2$). For the reverse transcription, the reaction mixture containing 5 µM RT primer, 0.5 mM dNTP mix, 50 µg/mL adenylated BSA, 5 mM DTT, 1 x first-strand buffer and 10 U/µL Superscript IV reverse transcriptase (Invitrogen) was prepared on ice. 30 µL of this mixture were added to the beads and the reactions were incubated at 40 °C for 1 h. Then, dissociated hybrids of biotin–RNA and cDNA were rebound by addition of NaCl to a final concentration of 1.5 M and incubation at 20 °C, 1,000 rpm for 1 h. Thereafter, reactions were centrifuged at 17,000 x *g*, rt for 1 min. The supernatants were discarded, and the beads were washed with 0.25 x streptavidin wash buffer.

Removal of free primers by ExoI digest

The streptavidin beads were equilibrated, blocked, and subsequently washed in the same manner as described above with 1× Exonuclease I buffer (670 mM glycine-KOH pH 9.5, 67 mM $MgCl_2$, 100 mM 2-mercaptoethanol). For the ExoI digest, the ExoI reaction mixture containing 1 x ExoI buffer and 1 U/µL ExoI (NEB) enzyme was prepared. 30 µL of this mixture were added to the beads and the reactions were incubated at 37 °C for 30 min. After 30 min of incubation, 1.5 µL of ExoI enzyme were added and reactions were incubated for another 20 min. Then, reactions were centrifuged at 17,000 x *g*, rt for 1 min. The supernatants were discarded, and the beads were washed with 0.25 x streptavidin wash buffer.

Release of cDNA into solution by alkaline digest and precipitation

The streptavidin beads were washed with immobilization buffer. The alkaline digest was performed by addition of 100 µL 0.15 M NaOH to the beads and incubation at 55 °C for 25 min. The columns were centrifuged at 17,000 x *g*, rt for 1 min. The flow-throughs were collected in 1.5 mL Eppendorf DNA LoBind tubes. The beads were washed by addition of 100 µL RNase-free water and centrifugation at 17,000 x *g*, rt for 1 min. Both flow-throughs were combined and neutralized by addition of 25 µL 3 M sodium acetate. The cDNAs were precipitated in the presence of 40 µg glycogen molecular grade and 500 µL ice-cold ethanol at -20 °C overnight.

C-tailing of cDNA with TdT

cDNA was precipitated by centrifugation at 21,000 x *g*, 4 °C for 2 h. The cDNA pellets were resuspended in 19 µL terminal deoxynucleotidyl transferase (TdT) mixture, which contained 1 x TdT buffer (Thermo Fisher) and 1.25 mM CTP. Subsequently, 1 µL (20 U) TdT enzyme was added

to the mixtures which were incubated at 37 °C for 30 min, and then inactivated by incubation at 70 °C for 10 min.

Second adaptor ligation

Second adaptor ligation mixture was prepared on ice in an 80 µL scale in the presence of 1 x Standard ligation buffer, 5 µM each pre-annealed cDNA anchor fwd and rev, 10 µM ATP, 1.5 Weiss U/µL T4 DNA ligase HC (Thermo Fisher) and the 20 µL TdT reaction. The mixtures were incubated at 4 °C overnight, were inactivated by heating to 65 °C for 10 min and were precipitated by addition of 20 µL 3 M sodium acetate, 100 µL H_2O, 2 µL (40 µg) glycogen molecular grade and 500 µl 100 % ethanol and incubation overnight at -20 °C and subsequent centrifugation. cDNA pellets were dissolved in 30 µl RNase-free water.

Test PCRs for determination of required PCR cycles

Test PCRs on cDNA were performed in a 50 µL scale using 1.0 µL precipitated cDNA in the presence of 1 x High-Fidelity PCR MasterMix (NEB), 2 µM forward primer with native barcode and 2 µM reverse primer with native barcode. PCR products were analysed after 10, 12, 14, 16, 18, 20, 22 and 24 cycles by 2 % agarose gel electrophoresis. 15 PCR cycles were chosen for the final PCR settings.

Final PCR and native PAGE purification

Final PCRs on cDNAs were performed in a 100 µL scale using 2.0 µL precipitated cDNA in the presence of 1 x High-Fidelity PCR MasterMix (NEB), 2 µM forward primer with native barcode and 2 µM reverse primer with native barcode (e.g BC1 fwd and rev, Supplementary Table 2). 15 PCR cycles were performed. The PCR reactions were purified by 10 % native PAGE. dsDNA was visualized using the Typhoon scanner and the smear was excised above 150 bp. dsDNA was eluted from the gel material by incubation in 4-5 mL 0.3 M NaOAc pH 5.5 while shaking at 350 rpm, 20 °C overnight. Then, the eluates were filtered through small 0.45 µm filters by recurring centrifugation at 5,600 x *g*, for 1 min. Filtered dsDNAs were precipitated by adding 2.5 x volumes of ice-cold ethanol, incubating at -20 °C and centrifuging at 18,500 x *g* at 4 °C for 2 h. Supernatants were discarded, and dsDNA-pellets were air-dried for a few minutes and resuspended in 200 µL RNase-free water. dsDNAs were ethanol-precipitated again and dsDNA pellets were resuspended in 10 µL RNase-free water. DNA concentrations were measured using the Quantus Fluorometer and QuantiFluor dsDNA System (Promega). Equimolar amounts (~ 33 fmol) of each sample were pooled for the subsequent Nanopore sequencing. The final volume was reduced to 25 µL using a SpeedVac concentrator.

Nanopore sequencing of enrichment libraries

Sequencing libraries were generated with the SQK-LSK109 Ligation Sequencing kit (Oxford Nanopore Technologies) according to the manufacturer's guidelines starting with 390 fmol of

input dsDNA. Sequencing was performed on Flongle flow cells (R9.4.1 chemistry) on a MinION device. Sequencing data of biological duplicates and 6 time points each is available under BioProject PRJNA1073512.

NAD captureSeq data analysis

Nanopore sequencing data was basecalled using the guppy basecaller (version 6.1.3). Reads were demultiplexed and trimmed with Porechop (version 0.2.4, https://github.com/rrwick/Porechop). Quality control was performed using pycoQC (48). Full-length reads were subsequently detected and re-oriented, if the reads belonged to the reverse strand (classification) by Pychopper (version 2.5.0, https://github.com/epi2me-labs/pychopper). Classified or non-classified reads were subsequently mapped to the reference genomes of *E. coli* K12 (U00096.3, https://www.ncbi.nlm.nih.gov/nuccore/U00096.3), T4 phage (NC_00086.4, https://www.ncbi.nlm.nih.gov/nuccore/NC_000866.4) and 100 nt control RNA (spike-in, Supplementary Table S3) with minimap2 (version 2.21) (42). The resulting sam files were sorted, filtered for primary alignments and converted to bam files using samtools (version 1.7) (43). Reads mapping to features were counted using featureCounts (from subread package version 2.0.1) (49) allowing for multioverlapping reads and using the respective gff3 annotation files from NCBI as well as a self-composed annotation file for the 100 nt control RNA as reference annotations for the feature "gene". Reads were subjected to manual inspection in Integrative Genomics Viewer (IGV, version 2.13.0) (45).

Counted reads were further analyzed using R (version 4.1.2) using ggplot2 (version 3.3.5), dplyr (version 1.0.7), tidyverse (version 1.3.1), reshape (version 0.8.8) and VennDiagram (version 1.7.3). The custom script is available at https://github.com/MaikTungsten/PhageEpitranscriptomics.

For analysis of promoters of identified NAD-RNAs, the following approach was used. T4 phage promoter information was retrieved from PhiSite (http://www.phisite.org/main/index.php?nav=home). The information about *E. coli* promoters was collected from two sources: the EcoCyc scientific database (https://ecocyc.org) and an existing differential RNA sequencing (dRNA-seq) dataset (50). The promoter sequences were manually identified using IGV and were compared with the sources mentioned above. Then, collected promoter sequences were used to generate MEME promoter motifs (51).

dRNA-Seq library prep

Differential RNA-Seq (dRNA-Seq) was performed on total RNA from a single biological replicate including the time points t0, t4, t10 and t20 isolated as described above. dRNA-Seq library prep was conducted by vertis Biotechnologie AG. Briefly, RNA was fragmented by sonication, followed by treatment with polynucleotide kinase (NEB). Subsequently, half of the RNA was subjected to TEX treatment, whilst the other half was mock-treated. The RNA samples were polyA-tailed and 5'-PPP-ends were trimmed to 5'-P-ends via RNA 5'-polyphosphatase (Epicentre). First-strand

cDNA synthesis was performed using an oligo(dT)-adapter and M-MLV reverse transcriptase followed by high-fidelity PCR amplification of the cDNA using primers suitable for Illumina TruSeq sequencing. Resulting dsDNA was purified with Agencourt AMPure XP beads (Beckman Coulter Genomics) and analysed by capillary gel electrophoresis (Shimadzu MultiNA microchip electrophoresis system). Equimolar amounts of each sample were pooled and size fractionated yielding a size range of 200 – 600 bp. The final library pool was sequenced on an Illumina NextSeq 500 system using 75 bp read length. dRNA-Seq data is available under accession code GSE255091 at the GEO database.

dRNA-Seq data analysis

Data analysis was performed in a miniconda environment with Python 3.9. Data quality was confirmed using FastQC (version 0.11.9). Reads from fastq files were mapped to the reference genomes of *E. coli* K12 (U00096.3, https://www.ncbi.nlm.nih.gov/nuccore/545778205, accessed 10th October 2022) and T4 phage (NC_000866.4, https://www.ncbi.nlm.nih.gov/nuccore/nc_000866.4, accessed 10th October 2022), which were retrieved from NCBI database, using the READemption pipeline (version 2.0.3) at standard settings (52). Alignments were converted to wiggle files using the coverage function of READemption (52).

Wiggle files from READemption pipeline were used as input for transcription start site prediction with Annogesic (Docker image retrieved 15th November 2022 from https://hub.docker.com/r/silasysh/annogesic/), which makes use of TSS predator (53,54). In order to optimize the prediction parameters, transcription start site annotations of *E. coli* U00096.3 were retrieved from RegulonDB (accessed 13th November 2022, https://regulondb.ccg.unam.mx/menu/download/datasets/index.jsp) and the TSSs from the first 200,000 genomic bases were gathered in a gff3 annotation file. The reference TSS file and the wiggle files for *E. coli* K12 and t0 were used to run TSS optimization with Annogesic at standard settings. The optimized prediction parameters were used to predict TSSs for all time points for T4 phage and *E. coli* wiggle files.

Comparison of dRNA-Seq and NAD captureSeq data

TSSs of NAD-capped transcripts called by the parameters mentioned above were retrieved from alignments in IGV and gathered in a gff3 file for T4 phage and *E. coli* separately. A custom R Script (R version 4.2.1) was compiled to search for the nearest TSS (within +/- 8 bp window), respectively, generated by TSS prediction based on the dRNA-Seq data. The custom script is available under https://github.com/MaikTungsten/PhageEpitranscriptomics.

NAD-capping of purchased RNAs *in vitro*

Capping reactions were performed in a 50 µL scale using 40 µM 5'-P-RNA-Cy5 (Supplementary Table S3), 50 mM $MgCl_2$ and approx. 5 mg of imidazolide nicotinamide mononucleotide (Im-

NMN) as previously described (55). Reactions were purified by centrifugation at 14,000 x *g*, 4 °C in 0.5 mL 3 kDa Amicon filters and washing with four column volumes of RNase-free water. RNAs were eluted in a final volume of 50 µL and stored at – 20 °C. RNA concentrations and NAD-capping efficiencies were determined by 20 % PAGE or 20 % APB-PAGE analysis using unmodified input RNA as a reference and ImageLab 6.1 for quantification of band intensities. NAD-capping efficiencies accounted for around 50 %.

Synthesis of ^{32}P-labelled NAD

500 µM nicotinamide mononucleotide (NMN), 10 mM DTT, 1 µCi/µL alpha-^{32}P-ATP, 1 x degradation buffer and 2.14 µM NadR (self-purified) were incubated at 37 °C for 1 h. The reaction was purified by P/C/I extraction and monitored by thin layer chromatography (TLC) using a 60:40 mixture of 100 % ethanol and 1 M NH_4OAc, pH 5 as mobile and Alugram TLC plates (Macherey Nagel) as stationary phase.

Cloning of vectors for protein expression

The *nudE.1* (GeneID: 1258692; UniprotID: P32271, Suplementary Table S2) was amplified from T4 phage DNA by high-fidelity PCR using forward and reverse primers introducing sites for restriction-based cloning as indicated in Supplementary Table S2. PCR products, purified via QIAQuick PCR purification kit (Qiagen), and pET28a vector, purified via GeneJet Plasmid Mini Prep Kit (Thermo Fisher), were both digested with NcoI and XhoI (both Thermo Fisher) and purified via PCR purification or gel extraction kit (both Qiagen). Vector and insert were ligated using T4 DNA ligase (Thermo Fisher) according to manufacturer's instructions and ligation products transformed into chemically competent *E. coli* BL21 DE3 cells. Plasmids isolated from clones were validated for correct insert via Sanger sequencing (Microsynth Seqlab) and finally transformed into chemically competent *E. coli* BL21 DE3 cells again for protein expression (Supplementary Table S4).

A similar workflow was employed for site-directed mutagenesis of plasmids replacing the restriction-based approach with a primer-driven site-specific mutagenesis approach with 5'-monophosphorylated primers by PCR amplification and re-ligation of the PCR product with mutation. The plasmids containing the mutations in the insert were retrieved as described above.

Expression and purification of proteins

Proteins were expressed from the respective plasmid (Supplementary Table S1, S4) in *E. coli* BL21 DE3. Cells were grown in LB medium at 37 °C, 180 rpm to an OD_{600} of 0.8, when protein expression was induced by addition of Isopropyl-beta-D-thiogalactoside to a final concentration of 1 mM. Bacteria were pelleted after incubation at 37 °C for 3 h. Pelleted bacteria were resuspended in Ni-NTA buffer A (50 mM Tris-HCl, pH 7.5, 1 M NaCl, 1 M urea, 5 mM $MgSO_4$, 5 mM β-mercaptoethanol, 5 % glycerol, 5 mM imidazole, one tablet complete EDTA-free protease inhibitor cocktail (Roche) per L) and lysed by sonication (2 x 5 min at 80 % amplitude, 0.5 s pulse). The

lysate was cleared by ultra-centrifugation at 37,000 x *g*, 30 min, 4 °C and the supernatant was filtered through 0.45 µm filters. Proteins were purified from the supernatant by Ni-NTA affinity chromatography using either Ni-NTA agarose beads (Jena Bioscience, for gravity-based purification) or 1 mL Ni-NTA HisTrap column (GE Healthcare, for fast performance liquid chromatography (FPLC)-based purification). Proteins were eluted either with Ni-NTA buffer B (with 300 mM imidazole added, gravity-based) or a gradient using Ni-NTA buffer B (FPLC-based) and analysed by SDS-PAGE. An NGC system (Bio-Rad) was used for all FPLC-based protein purifications.

Proteins were further purified by size-exclusion chromatography (SEC) using a Superdex 200 10/300 GL column (GE Healthcare) integrated in the NGC system. SEC buffer containing 300 mM NaCl and 50 mM Tris-HCl, pH 7.5 was used as running buffer. Fractions of interest were analysed by SDS–PAGE, pooled and concentrated in Amicon Ultra-4 centrifugal filters (molecular weight cut-off (MWCO) 10 kDa with centrifugation at 5,000 x *g*, 4 °C). Protein concentration was measured with a NanoDrop ND-1000 spectrophotometer (Thermo Fisher). Finally, proteins were stored in SEC buffer supplemented with 50 % glycerol at -20 °C. For the estimation of the oligomeric state of the proteins, 150 µL protein analysed on a Superdex 200 10/300 GL column (GE Healthcare) integrated in an NGC system via constant flow of SEC buffer with known monomeric proteins serving as calibration standards. Python package seaborn was used to perform linear regression of calibration standards and estimate the oligomeric state of analysed proteins.

AlphaFold2 prediction of NudE.1

The protein sequences of *nudE.1* WT (Supplementary Table S3) were used to predict structures via the Google Colab Tool of AlphaFold2 – named ColabFold (version 1.5.2, access date 20th June 2023) (56). Standard settings were applied expecting NudE.1 to occur as a monomer. Prediction from rank 1 was further analysed each in PyMol (version 2.4.1).

In vitro decapping and hydrolysis assays

500 nM NAD-capped RNA-Cy5 (Supplementary Table S3) were incubated in the presence of 1 mM DTT, 1 x degradation buffer (12.5 mM Tris-HCl pH 7.5, 25 mM NaCl, 25 mM KCl, 5 mM $MgCl_2$) and either 25 nM NudE.1 WT or NudE.1 E64,65Q or NudC WT (NEB). For NAD spike-in kinetics, NAD was included in the reaction at final concentrations of 350 µM (700-fold molar excess over NAD-RNA) or 750 µM (1,500-fold molar excess over NAD-RNA) and a spike-in of radioactive ^{32}P-NAD (if indicated, 2.6 nM). Reactions were incubated at 37 °C and samples taken throughout time-course of the reaction were immediately stopped by addition of one volume 2 x APB loading dye (8.3 M urea, 0.05 % (w/v) bromophenol blue, 0.05 % (w/v) xylene cyanol). A sample was taken before addition of enzyme each. Samples were analyzed by 20 % APB-PAGE and gels were imaged at ChemiDoc (Bio-Rad) using the Cy5 channel. Reactions using ^{32}P-NAD were stopped by heating samples at 90 °C for 1 min and were subsequently analysed by TLC. TLC plates were imaged by

autoradiography using a Typhoon Imager (Amersham Biosciences). Intensity-based band quantification was performed in ImageLab (Bio-Rad).

NAD only hydrolysis assays were performed using the same settings with the following abberations. A final concentration of 25 µM NAD and a spike-in of radioactive ^{32}P-NAD (2.6 nM) were used instead of NAD-RNA-Cy5 in the presence of 1 µM NudE.1 WT or NudE.1 E64,65Q or NudC WT. Reactions were analysed by TLC and autoradiography as described above.

Determination of cellular metabolite/cofactor levels

Cultures were quenched by adding 1 mL culture to 1 mL 70 % methanol at -80 °C and harvested by centrifugation at 13,000 x *g*, -5 °C, 5 min. Supernatant was carefully removed and pellets stored at -80 °C. Intracellular metabolites were extracted adding a mixture of 50 % methanol and 50 % TE buffer pH 7 (10 mM Trizma base and 1 mM EDTA)) at -20 °C to the frozen cell pellets. The volume of extraction fluid per cell was kept constant throughout all experiment by adjusting it according to the amount of cells in each pellet (volume per pellet calculated according to OD_{600} measurement). For membrane desintegration, an equal volume of -20 °C chloroform was added to each pellet, pellets were resuspended by vortexing, and extraction was performed by shaking at 4 °C, 1,000 rpm for 2 h. Organic and aqueous phase were separated by centrifugation at 21,000 x *g*, -10 °C for 10 min and aqueous upper phase was filtered through 0.2 µm PFTE filters (Phenomenex) and stored at -80 °C until analysis.

Quantitative determination of NAD, FAD, and UDP-GlcNac was performed using a LC-MS/MS. Chromatography was performed on an Agilent Infinity II 1290 HPLC system using a SeQuant ZIC-pHILIC column (150 × 2.1 mm, 5 µm particle size, peek coated, Merck) connected to a guard column of similar specificity (20 × 2.1 mm, 5 µm particle size, Phenomenex) at a constant flow rate of 0.1 mL/min with mobile phase composed of fractions of buffer A (10 mM ammonium acetate in water, pH 9, supplemented with 5 µM medronic acid) and buffer B (10 mM ammonium acetate in 90:10 acetonitrile to water, pH 9, supplemented with 5 µM medronic acid) at 40 °C.

2 µL sample were injected. The mobile phase profile consisted of the following steps of linear gradients: 0 – 1 min constant at 75 % B; 1 – 6 min linear gradient from 75 to 40 % B; 6 to 9 min constant at 40 % B; 9 – 9.1 min linear gradient from 40 to 75 % B; 9.1 to 20 min constant at 75 % B. An Agilent 6495 ion funnel mass spectrometer was used in negative and positive ionisation mode with an electrospray ionization source and the following conditions: ESI spray voltage 3500 V, nozzle voltage 1000 V, sheath gas 300 °C at 9 L/min, nebulizer pressure 20 psig and drying gas 100 °C at 11 L/min. Compounds were identified based on their mass transition and retention time compared to standards (Supplementary Table 5). Chromatograms were integrated using MassHunter software (Agilent). Absolute concentrations were determined based on an external standard curve.

According to our Coulter counter measurement an average *E. coli* culture at an OD_{600} of 0.8 contains 3 * 10^8 cells per 1 mL ($cells_{per\ extraction\ volume}$). Applying an average single cell volume (V_{cell}) of 1 fL per cell (57,58), the intracellular volume of all cells in a pellet derived from 1 mL of sample at an OD of 0.8 thus amounts to 3 * 10^8 fL (=3 * 10^{-7} L). As all metabolites detected in the extract are derived from that volume, the intracellular concentration can be calculated by determining the amount of metabolites in the extract ($V_{extract}$ * $c_{metabolite}$) using a correction factor of 10^{-12} to yield a molar concentration and divided by the intracellular volume of all cells in the pellet (prior to extraction). Thus, the concentration of each metabolite per cell ($c_{per\ cell}$ [M]) can be calculated with equation *2*:

$$c_{per\ cell}[M] = \frac{c\ [\mu M] * 10^{-12} * extraction\ volume\ [\mu l]}{cells\ in\ extraction\ volume * volume\ per\ cell} \qquad (2)$$

LC-MS analysis of NAD-caps in total RNA

Total RNAs were washed using 0.5 mL 3 kDa spin filters by centrifugation at 14,000 x *g*, 18 °C. 200 µg total RNA were heated at 90 °C for 3 min and washed once with 8.3 M urea (at 90 °C), followed by two washing steps with 8.3 M urea (at room temperature), one washing step with Millipore water, two washing steps with 4.15 M urea and four washing steps with Millipore water. RNA was recovered by washing the filter four times with 200 µL Millipore water. RNA was concentrated using vacuum concentration and RNA concentration determined at NanoDrop.

40 µg of total RNA were hydrolyzed by a two-step protocol using first 0.1 U nuclease P1 and 0.1 U phosphodiesterase 1 in the presence of 2.5 mM ammonium acetate pH 5.3 and 0.2 mM $ZnCl_2$ at 37 °C for 2 hours. The resulting nucleotides were dephosphorylated by addition of 2 U calf intestine phosphatase and Tris-HCl pH 8 to a final concentration of 5 mM and incubated for another hour at 37 °C. (Note: enzymes should not be dissolved in glycerol stocks, as ribo-nicotinamide signals experience severe ion suppression in glycerol-containing hydrolysates.) As an internal standard (SILIS) *E. coli* total RNA with complete carbon-13 labelling (59) was digested as described above and co-injected into the LC-MS.

For NAD-cap quantification, an Agilent 1290 Infinity II equipped with a diode-array detector (DAD) combined with an Agilent Technologies G6470A Triple Quad system and electrospray ionization (ESI-MS, Agilent Jetstream) was used.

Nucleosides were separated using a Synergi Fusion-RP column (Synergi® 2.5 µm Fusion-RP 100 Å, 150 × 2.0 mm, Phenomenex®, Torrance, CA, USA). LC buffer consist of 5 mM NH4OAc pH 5.3 (buffer A) and pure acetonitrile (buffer B) were used as buffers. The gradient starts with 100% buffer A for 1 min, followed by an increase to 10% buffer B over a period of 4 min. Buffer B is then increased to 40% over 2 min and maintained for 1 min before switching back to 100% buffer A over a period of 0.5 min and re-equilibrating the column for 2.5 min. The total time is 11 min and the flow rate is 0.35 mL/min at a column temperature of 35 °C.

An ESI source was used for ionization of the nucleosides (ESI-MS, Agilent Jetstream). The gas temperature (N2) was 230 °C with a flow rate of 6 L/min. Sheath gas temperature was 400 °C with a flow rate of 12 L/min. Capillary voltage was 2500 V, skimmer voltage was 15 V, nozzle voltage was 0 V, and nebulizer pressure was 40 Psi. The cell accelerator voltage was 5 V. For quantification, a DMRM and positive ion mode was used (Table 1).

Table 1: MS parameters for quantification of canonical nucleosides and ribo-nicotinamide (r-NA).

	Rt [min]	m/z precursor	m/z product
A	5,3	268,1	136
A SILIS	5,3	278	141
C	1,8	244,1	112
C SILIS	1,8	253	116
G	4,2	284,1	152
G SILIS	4,2	294	157
r-NA	1,5	255,1	123
rNA SILIS	1,5	266,2	129
U	2,9	245,1	113
U SILIS	2,9	254	117

For calibration, synthetic nucleosides were weighed and dissolved in water to a stock concentration of 1-10 mM. 2.5 mM ribo-nicotinamide (r-NA) was prepared from a 10 mM NADP solution hydrolyzed with NP1 and phosphatase as described for the sample preparation above (phosphodiesterase was omitted). Calibration solutions ranged from 5 pmol to 5000 pmol for each canonical nucleoside and from 0.5 pmol to 500 pmol for ribo-nicotinamide (r-NA). Analogous to the samples, *E. coli* ^{13}C-SILIS was co-injected with each calibration. The calibration curve and the corresponding evaluation of the samples were performed using Agilent's qualitative MassHunter software. All modification abundances were normalized to the amount of RNA injected using the sum of all canonicals.

CircNC-like protocol for NAD-RNA validation

The circNC-like protocol was conducted similar as described by Sharma and colleagues (60). In a 100 µL scale, 8 µg total RNA from *E. coli* JM109 + pUC19 or *E. coli* B strain was dephosphorylated with 0.4 U/µL QuickCIP (NEB) in 1 x rCutSmart buffer (NEB) at 37 °C for 1 h. The RNA was purified using the Zymo RNA Clean and Concentrator kit eluting the RNA in 15 µL. Subsequently, 4 µL dephosphorylated RNA were subjected to NudC treatment by incubation in the presence of 1 mM DTT, 1 x degradation buffer (see composition above) and 1.5 µM NudC (or an equivalent volume of RNase-free water as negative control) in 50 µL scale at 37 °C for 1 h. A non-enzyme sample serves as negative control. RNA was then purified again and the eluate was subjected to

circularization with T4 RNA Ligase 1 (NEB). Briefly, 15 µL RNA was incubated in the presence of 10 % PEG8000, 0.5 U/µL T4 RNA Ligase 1, 1 U/µL murine RNase inhibitor (NEB), 50 µM ATP and 1 x RNA ligation buffer (NEB) at 25 °C for 16 h. RNA was purified again and concentration determined at NanoDrop. 50 ng purified RNA was then subjected to reverse transcription with Superscript IV (Invitrogen) according to manufacturer's instructions using 100 nM RNA-specific reverse transcription primer followed by RNase H digest with 5 µL RNase H (NEB) at 37 °C for 20 min. 1 µL of RT reaction were used as template for qPCR in 10 µL scale and technical duplicates per sample with iTaq Universal SYBR Green Supermix (Bio-Rad). Log2 Fold Changes were calculated as the difference between the cq-value of the control sample and the NudC WT treated sample.

Data visualization and statistics

If not indicated otherwise, statistical tests and plots were performed with R (version 4.2.2) using ggplot2 (version 3.4.1) and ggpubr (version 0.6.0).

RESULTS

The NAD-RNA pool is dynamically reshaped during T4 phage infection

NAD-RNAs have been reported to exist in exponentially growing *E. coli* (5,10). Phages most efficiently infect their bacterial hosts during exponential growth phase (61). Therein, nucleotides, ribosomes and RNAP are highly abundant allowing for efficient reproduction (62,63). When T4 phage infects *E. coli*, the host transcriptome is rapidly modulated alongside dynamic phage gene expression (34). It stands to debate, whether infection induces changes in the host's NAD-RNA pool and whether even T4 phage transcripts are NAD-capped. Moreover, mechanisms that result in the dynamic regulation of NAD-RNAs upon phage infection are currently uncharacterized.

In order to comprehensively determine the occurrence of both NAD-capped host and phage transcripts during infection, we made use of the NAD captureSeq technology (5,47). To sequence full-length NAD-RNAs, we implemented SPAAC in our NAD captureSeq approach by using 3-azido-propanol as substrate for the ADP-ribosyl cyclase (ADPRC) and biotin-dibenzocyclooctyne (DBCO) for the subsequent biotinylation by SPAAC (9,10) (Figure 1). Further, in order to sequence full-length NAD-capped transcripts, we introduced a custom barcoding PCR in the final amplification of the resulting cDNA. This can be subjected in a multiplexed fashion to Oxford Nanopore sequencing using an affordable Flongle flow cell (~ 175 € for one sequencing experiment) (Figure 1). We included a 100 nt control NAD-RNA (Supplementary Table S3) from the beginning of the NAD captureSeq workflow to monitor the success of the extensive capture and sequencing protocol.

We applied our NAD captureSeq pipeline to comprehensively determine the occurrence of NAD-RNAs before (t0) and during T4 phage infection (1, 4, 7, 10, 20 min post infection) (Supplementary Figure S1). By sequencing 12 samples per replicate on individual Flongle flow cells (6 time points, in the presence (+) and without (minus) ADPRC per time point) we obtained 220,028 (R1) or 499,383 (R2) pass reads, respectively (Supplementary Figure S2). After demultiplexing, we gained an average number of 14,777 or 36,255 reads per barcode (sample), respectively.

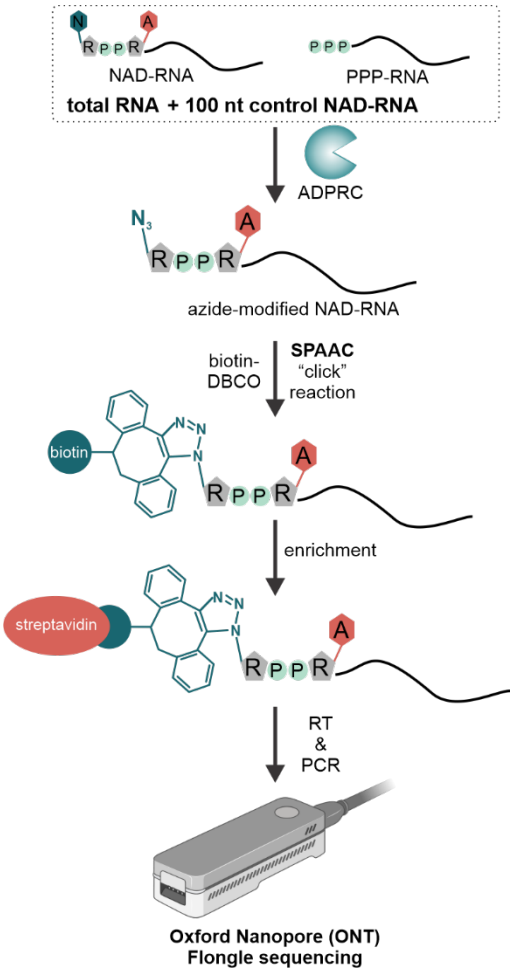

Figure 1: Adjusted NAD captureSeq workflow for the detection of NAD-capped RNAs.
Schematic illustration of the optimized NAD captureSeq workflow. Total RNA with a spike-in of a 100 nt control NAD-RNA is subjected to treatment with ADPRC yielding azide-modified NAD-RNAs. These are subsequently linked to DBCO-biotin using SPAAC chemistry. Biotin-modified RNAs are captured on a streptavidin resin, reverse transcribed, PCR amplified and finally sequenced on a Nanopore Flongle flow cell.

We measured enrichment of the 100 nt control NAD-RNA in both replicates and all time points (Figure 2A,B, Supplementary Table S6A,B, Supplementary Figure S3, S4) indicating that our NAD captureSeq workflow successfully captured NAD-RNAs in all samples. *E. coli* NAD-RNAs that we identified before infection (Figure 2A, Supplementary Table S6A,B, Supplementary Figure S3A, S4A) agree well with previously reported small regulatory RNAs (sRNAs) such as GcvB, McaS, GlmY or GadY or mRNAs such as from *acpP* or *aspA* genes (5,10). Further, we found several *E. coli* tRNA transcripts from the *valU-valX-valY* and *metZ-metW-metV* operons to be enriched in the +ADPRC sample (Figure 2A, Supplementary Table S6A,B, Supplementary Figure S3A,S4A). This was unexpected due to the post-transcriptional processing of tRNAs from an RNA precursor into mature tRNA molecules (64). Closer inspection of the read distribution at the respective tRNA loci demonstrated that tRNAs are NAD-capped as polycistronic precursor transcripts spanning the entire operon (Supplementary Figure S5). This exemplifies the power of the SPAAC- and ONT-based NAD captureSeq approach to enrich full-length NAD-capped transcripts or longer fragments thereof.

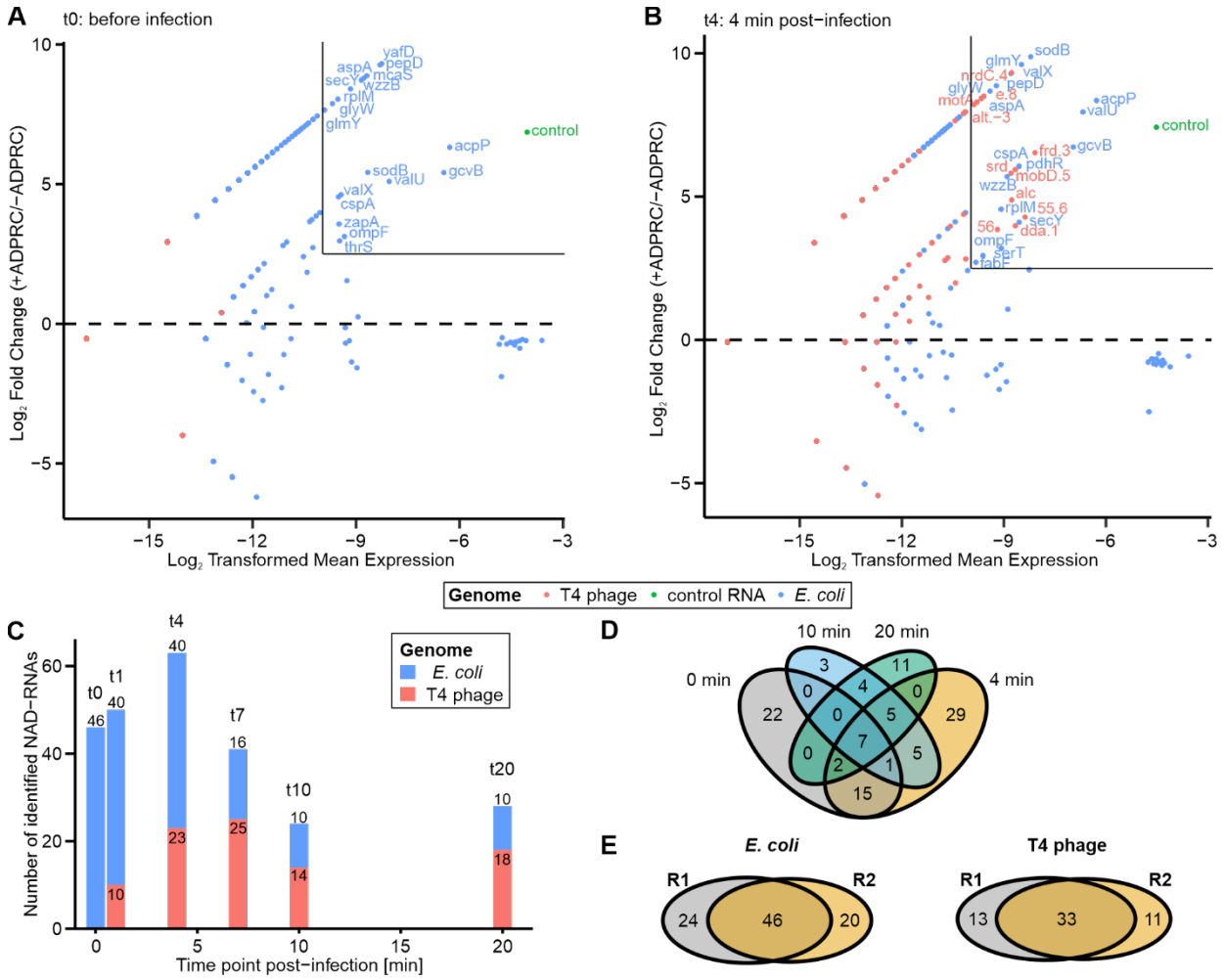

Figure 2: Identification of NAD-RNAs using time-resolved dual NAD captureSeq.
(**A**, **B**) MA (log ratio, mean average) plots showing enrichments of NAD-capped RNAs before infection (t0, **A**) and 4 min post infection (t4, **B**) for replicate 1 at an MOI of 1.5 (Supplementary Figure S1B). y-axis represents the log2 fold change in normalized read counts comparing fully-treated sample (+ADPRC) and negative control (-ADPRC), x-axis shows log2 transformed mean normalized read counts for genes from + and –ADPRC samples. Plots for all time points and replicates are shown in Supplementary Figures S2 and S3. (**C**) Bar plot depicting the number of NAD-RNAs over the time course of infection per entity as identified by time-resolved NAD captureSeq for replicate 1. (**D**) Distribution of NAD-RNAs across different infection phases for replicate 1. (**E**) Distribution of *E. coli* and T4 phage NAD-RNAs identified in different replicates.

Next, we set out to investigate the changes in the NAD-cap epitranscriptome during T4 phage infection. Previous studies have shown that the host (*E. coli*) transcriptome is rapidly degraded upon infection, while T4 phage genes are expressed in a temporally tightly-regulated manner (33,34). Early during infection, genes for host takeover and control are transcribed, followed by middle genes for DNA replication and late genes involved in phage assembly and host cell lysis (33,34). We made similar observations for the NAD-cap epitranscriptome during T4 phage infection. First, the number of identified *E. coli* NAD-RNAs decreases over the time-course of infection (Figure 2C) ranging from 46 RNAs before infection to only 10 RNAs 20 min post infection.

In parallel, throughout infection, T4 phage NAD-capped RNAs vary in their number and identity. Predominantly, T4 phage mRNAs appear to be NAD-capped. The functions of NAD-RNAs vary with the respective infection phase. Early NAD-capped RNAs play roles in host takeover, whilst middle and late T4 NAD-RNAs are encoded by genes for DNA replication or structural phage proteins, respectively (Supplementary Table S6A,B). This demonstrates the dynamic nature of the NAD-cap epitranscriptome during T4 phage infection. Sequence analysis of the identified NAD-RNAs yielded two distinct features. For one, NAD-RNAs share a 5′-adenosine – a prerequisite for RNAP-mediated NAD-capping (5,22). Also, for some NAD-capped T4 mRNAs we detected a Shine Dalgarno sequence within the 50 nt downstream the 5′-end indicating that they have a coding function and could possibly be translated.

A total of 5 *E. coli* NAD-RNAs are found across all time points and replicates (Table 2). These *E. coli* NAD-RNAs encompass two sRNAs, GcvB and GlmY, two mRNAs encoding SodB and AcpP proteins, and the *valU* tRNA precursor (Table 2). These transcripts fulfil various functions ranging from regulation of amino acid metabolism (GcvB) (65), fatty acid biosynthesis (*acpP*) (66) to protection from oxidative stress (*sodB*) (67). Dual RNA-Seq has previously identified the sRNA GlmY, a regulatory RNA involved in, for instance, response to cell envelope stress (68), to be stable throughout T4 phage infection, while the abundance of the other four transcripts declines throughout infection (34). Thus, host NAD-RNAs can be both stable and instable transcripts during infection. In contrast to the set of continuously detected *E. coli* NAD-RNAs, T4 NAD-RNAs are only shared by two or three adjacent time points of infection or are unique for one time point (Figure 2D, Supplementary Table S6A,B). The T4 protein-coding genes *dda.1*, *srd*, *56*, *55.6* and *frd.3* encode the most abundant T4 phage NAD-RNAs (based on detection in both replicates and highest mean expression) (Table 2). Most of the proteins encoded by these NAD-RNAs are functionally uncharacterized except for Srd that induces RNase E-mediated RNA decay (69) and 56 that is part of a complex for nucleotide dephosphorylation (70). Importantly, these abundant T4 phage NAD-RNAs do not belong to the top 10 most highly expressed T4 genes at any time point of infection as indicated by existing RNA-Seq data (34). Thus, the detection of these NAD-RNAs does not result from the general high abundance of these transcripts during T4 phage infection.

To determine the robustness of the NAD captureSeq workflow, we compared the *E. coli* and T4 phage NAD-RNAs that were overall identified in both replicates. We recorded a good overlap between both replicates (Figure 2E), indicating that most NAD-RNAs are reproducibly detected. Finally, we validated our data by performing qPCR on the cDNAs used for final library amplification and sequencing. We recorded enrichments for NAD-RNAs in the +ADRPC-sample compared to the minus-ADPRC control as reflected in the NAD captureSeq data (Supplementary Table S7).

These data provide the first comprehensive insights into the dual NAD-cap epitranscriptome of the T4 phage and its host *E. coli*. The identified NAD-RNAs are in agreement with the infection

phase-specific expression of T4 phage genes and the overall degradation of host transcripts and indicate a dynamic regulation of the NAD-RNA pool during T4 phage infection.

Table 2: Abundant *E. coli* and T4 phage NAD-RNAs identified by NAD captureSeq.

Abundant *E. coli* NAD-RNAs during infection		
Gene	**RNA type, occurrence**	**Function**
gcvB	sRNA, entire infection	regulation of amino acid metabolism (65)
glmY	sRNA, entire infection	response to cell envelope stress (68); regulation of GlmZ (71); stable during T4 phage infection (34)
acpP	mRNA, entire infection	acyl carrier protein in fatty acid biosynthesis (66)
sodB	mRNA, entire infection	protection from oxidative stress (67)
valU	valine-tRNA, entire infection	valine-tRNA
Most abundant T4 phage NAD-RNAs		
Gene	**RNA type, occurrence**	**Function**
dda.1	mRNA, middle to late phase	uncharacterized protein
srd	mRNA, middle to late phase	inducer of RNase E-mediated RNA decay (69)
56	mRNA, early to middle phase	involved in a protein complex for nucleotide dephosphorylation (70)
55.6	mRNA, early to middle phase	uncharacterized protein
frd.3	mRNA, early phase	uncharacterized protein

Validation of NAD-capped phage and host transcripts

In order to obtain qualitative proof for the NAD-RNAs identified by NAD captureSeq, we employed a ligation-based assay to verify specific NAD-RNAs of interest – similar to circNC (60) In brief, this method includes the removal of all phosphates from uncapped RNAs, whilst leaving NAD-capped RNAs intact. Subsequently, the cleavage by NudC generates 5'-P-RNAs from NAD-RNAs only, which can then be circularized through RNA ligation (Figure 3A). After reverse transcription, a unique cDNA is created that is amplified by specific primers in a qPCR. We first executed this workflow on RNA from *E. coli* JM109 + pUC19 that contains NAD-capped RNAI (5). Upon qPCR comparing both a NudC- and a mock-treated sample, we detected a difference in cq values of 3.5 (Figure 3B). This corresponds to a log2 fold change of 3.5 comparing NudC- and mock-treated samples. Further, this demonstrates that the unique cDNA derived from NAD-capped RNAI is approx. 11-fold ($2^{3.5}$-fold) more abundant in the NudC-treated sample according to our expectations. Importantly, 5S rRNA, which is not NAD-capped as described before (5,10), was not found enriched in the NudC-treated sample compared to the control (Figure 3B).

Using this methodology, we validated that *E. coli* sRNA GcvB as well as T4 phage *dda.1* mRNA are indeed NAD-capped 7 minutes post infection (Figure 3B). We note, that we cannot conclude on their abundance relative to their 5′-triphosphorylated transcripts (PPP-RNA). Nevertheless, we provide essential proof for the existence of distinct NAD-RNAs that is independent from the NAD captureSeq workflow.

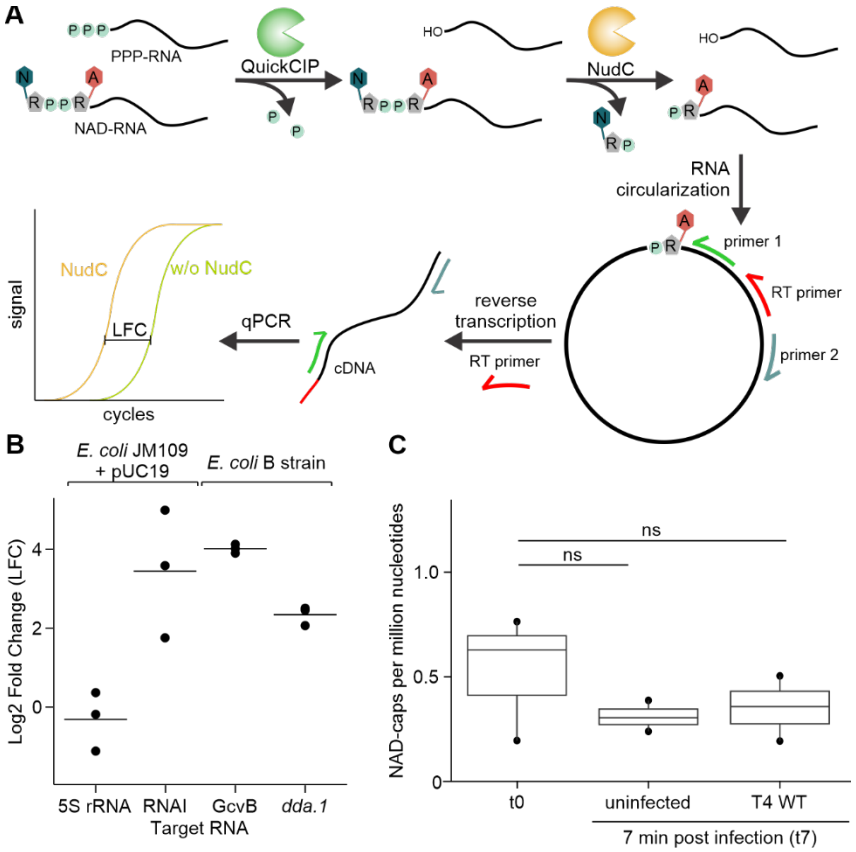

Figure 3: Validation of NAD-RNAs via a circNC-like assay and LC-MS.
(**A**) Ligation-based assay to prove the existence of specific NAD-RNAs. Briefly, total RNA is subjected to QuickCIP-treatment followed by NudC digest leaving a monophosphate only on formerly NAD-capped RNAs. RNA is then circularized by ligation and reverse transcribed with a target specific RT primer creating a unique cDNA spanning over the +1A position. The cDNA serves as a template for qPCR with target-specific primers to assess cDNA abundance in a NudC-treated and control sample as log2 fold change (LFC). (**B**) Log2 fold changes between control and NudC-treated total RNAs in qPCR targeting selected *E. coli* and T4 phage NAD-RNAs using our ligation-based assay (n=3). (**C**) NAD-cap levels in *E. coli* total RNA before infection (t0) and after 7 minutes (t7) in the absence of phage (uninfected) or in the presence of T4 phage as measured by LC-MS (n=3). NAD-cap levels are given as NAD-caps per million nucleotides, where 0.52 NAD-caps per million nucleotides correspond to approx. 1.56 fmol NAD-caps/µg total RNA. Boxplots indicate individual data points including their median. NAD concentrations before infection (t0) and 7 min post infection (t7) were compared using Welch two-sample t-test (p_{signif} < 0.05, ns: non-significant).

To validate the general existence of NAD-capped RNAs in *E. coli*, we employed LC-MS to determine NAD-cap levels in *E. coli* total RNA. We detected 0.53 NAD-caps per million nucleotides (corresponding to approx. 1.56 fmol NAD-caps/µg total RNA) in *E. coli* total RNA before infection (Figure 3C). This agrees well with previously reported 2.2 fmol NAD-caps/µg total RNA in *E. coli* (7). 7 minutes post infection, NAD-cap levels were identified at similar concentrations in uninfected *E. coli* (0.31 NAD-caps per million nucleotides) and T4 WT-infected *E. coli* (0.35 NAD-caps per million nucleotides) (Figure 3C). Thus, while we found dynamic modulation of the NAD-cap epitranscriptome already 7 min post infection (Figure 2C), overall NAD-RNA levels remain constant during infection. Moreover, this further validates the existence of both phage and host NAD-RNAs as identified by NAD captureSeq.

NAD-capping is performed by the host RNAP

The *E. coli* RNAP, which caps host NAD-RNAs *ab initio* during transcription (22), is also responsible for the transcription of T4 phage genes during infection (32). Thus, we supposed that T4 phage transcripts are analogously NAD-capped by the host RNAP. Therefore, we performed differential RNA-Seq (dRNA-Seq) (72-74) to determine the global transcription start sites (TSSs) in *E. coli* B strain before and at three time points of T4 phage infection. Thereby, we identified in total 5341 *E. coli* TSSs and 150 T4 phage TSSs including 22 phage antisense TSSs (Figure 4A,B, Supplementary Table S8A,B). The number of identified TSSs decreases for *E. coli* over the time course of infection (from 4830 TSSs (t0) to 2996 TSSs (t20)), whilst the number of T4 phage TSSs is increasing with no meaningful TSS identified prior to infection (Supplementary Table S8A,B). When comparing the positioning of the "canonical" TSSs to the TSSs of the NAD-RNAs identified by NAD captureSeq, we observed a good overlap for both *E. coli* and T4 phage NAD-RNAs (Figure 4C,D). The mean displacement of NAD-RNA to canonical TSSs accounted for 1.5 bp (R1) or 2.0 bp (R2) for *E. coli* NAD-RNAs or 3.3 bp (R1) or 3.0 (R2) bp for T4 phage NAD-RNAs, respectively (Figure 4E,F). Importantly, the TSSs of NAD-capped tRNA precursors (Supplementary Figure S5A,B) agree with the TSSs of these tRNA primary transcripts without any displacement.

The general *E. coli* promoter motif identified by dRNA-Seq is characterized by an AT-rich -10 element and predominant occupancy of the TSS by A or G (Supplementary Figure S6A). Among the *E. coli* NAD-RNA promoters only, a +1A TSS is shared (Figure 4E), which is an essential feature for *ab initio* NAD-capping of transcripts by the RNAP (5,22). Apart from that distinct feature of *E. coli* NAD-RNA promoters, they share the AT-rich -10 element and a T-rich -35 element with the *E. coli* consensus promoter identified here. The consensus T4 phage promoter also contains an AT-rich -10 element and displays a tendency towards +1A TSSs (Supplementary Figure S6B) in agreement with the previously studied T4 promoter motif (32). 60 % (90 in total) of the T4 phage promoters identified here initiate with adenosine. For 63 % of these promoters, we identified NAD-RNAs by NAD captureSeq. Similar as for *E. coli* NAD-RNA promoters, T4 NAD-RNA promoters share the +1A TSS and the AT-rich -10 element, too (Figure 4F). Interestingly, a comparison to our

T4 consensus promoter indicates enrichment of thymine at -35 position and a GTG motif downstream of the -10 element. The -35 element of strong promoters is typically AT-rich to enable the binding of the RNAP and efficient transcription (75). Importantly, the features of the T4 NAD-RNA promoters are not enriched among the 90 T4 phage +1A promoters (Supplementary Figure S6C). Thus, these distinct promoter elements may drive NAD-capping of the observed set of T4 phage NAD-RNAs during infection.

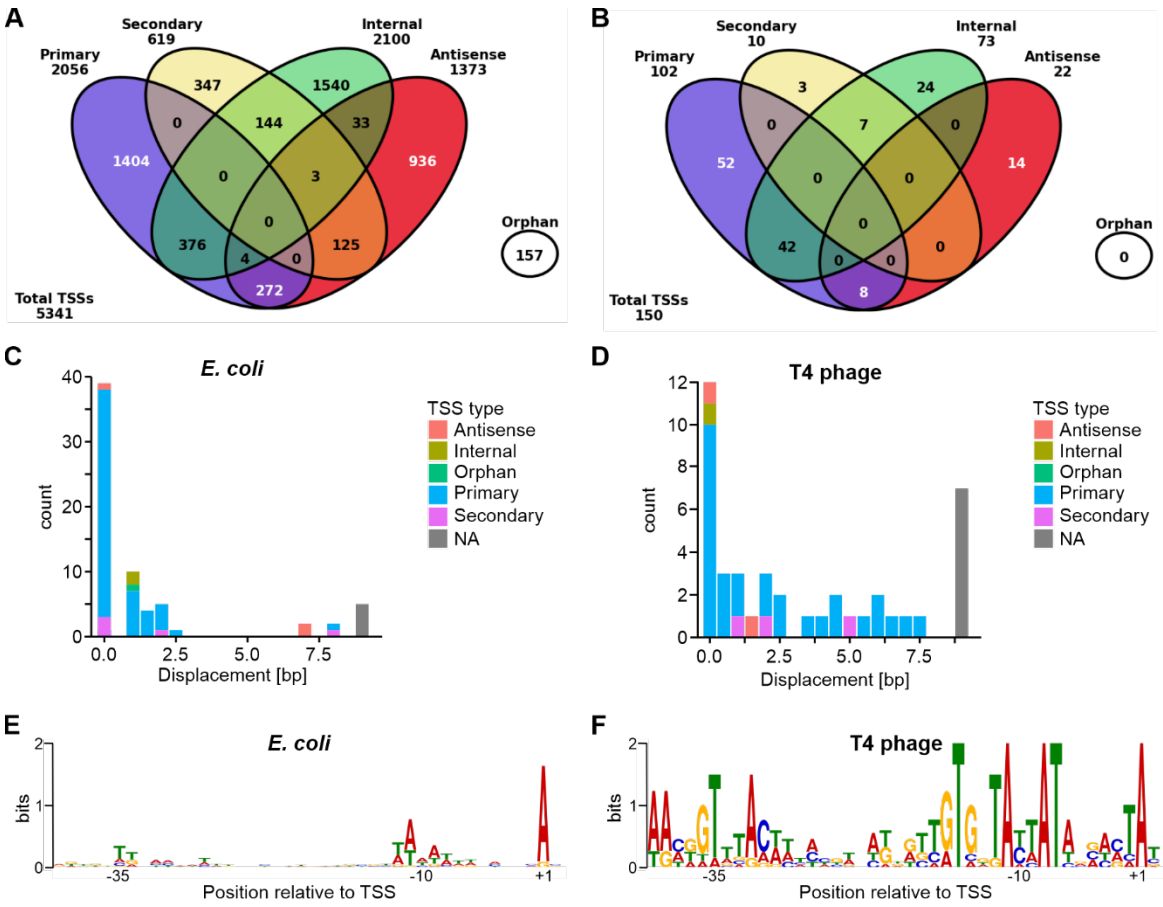

Figure 4: Global transcription start site (TSS) and NAD-RNA TSS analysis in *E. coli* and T4 phage. (**A**, **B**) Types and distribution of all transcription start sites (TSSs) in *E. coli* (**A**) and T4 phage (**B**) during infection as revealed by time-resolved dual differential RNA-Seq (dRNA-Seq) during T4 phage infection of *E. coli* before (0 min) and 4, 10, 20 min post-infection (n=1). (**C**, **D**) Displacement of TSSs of NAD-RNAs identified by NAD captureSeq from "canonical" TSSs derived from dRNA-Seq data for *E. coli* (**C**) and T4 phage (**D**) NAD-RNAs from replicate 1. (**E**, **F**) Motifs of promoters of all identified *E. coli* (89 promoters) (**E**) and T4 phage (42 promoters) (**F**) NAD-RNAs including the TSS (+1) and the -10 and -35 element. Motifs were created using Meme Suite (51).

In conclusion, we provide evidence – in agreement with the known biosynthesis mechanism of NAD-RNAs – that NAD-capping during T4 phage infection is performed by the *E. coli* RNAP by

initiating transcription with NAD. TSSs of primary and NAD-capped transcripts are overlapping for both phage and host. Promoter sequences of both phage and host NAD-RNAs indicate +1A TSSs as an expected requirement for NAD-capping. Further, T4 phage promoters may harbor additional regulatory sequences that could orchestrate NAD-capping of the observed subset of T4 phage transcripts. In addition, this demonstrates the power of dual-dRNA-Seq to complement the findings from our dual NAD captureSeq approach.

The T4 phage Nudix hydrolase NudE.1 hydrolyses NAD-caps *in vitro*

In *E. coli*, degradation of NAD-RNAs is initiated by NAD-RNA decapping by the Nudix hydrolase NudC (8,24). We wondered whether additional Nudix hydrolases may play a role in NAD-RNA decapping during T4 phage infection. The T4 phage encodes one Nudix hydrolase – termed NudE.1 – that has been described to hydrolyze adenosine-derived cofactors and metabolites, primarily ADP-ribose, Ap_3A and FAD, within their pyrophosphate moiety (37). Notably, no activity of NudE.1 on NAD was reported (37).

We used AlphaFold2 (56) to predict the structure of NudE.1, which reveals a wide-open cleft in which the catalytically relevant Nudix motif is located (Figure 5A, Supplementary Figure S7A,B). Based on this potential active site conformation, we speculated that NudE.1 may also accept substrates such as NAD and NAD-RNA for hydrolysis. We expressed and purified NudE.1 migrating as an apparent monomer during size exclusion chromatography (Supplementary Figure S7C). Initially, we assessed the activity of NudE.1 on NAD using site-specifically ^{32}P-labelled NAD. We observed that NudE.1 efficiently hydrolyses NAD into nicotinamide mononucleotide (NMN) and AMP, whilst a mutant of the catalytic site E64,65Q (NudE.1 E64,65Q) did not show hydrolysis activity on NAD (Figure 5B). Notably, NudC hydrolyses NAD less efficiently at the same substrate and enzyme concentrations indicating NudE.1 as a more efficient Nudix hydrolase under these conditions *in vitro* (Figure 5B).

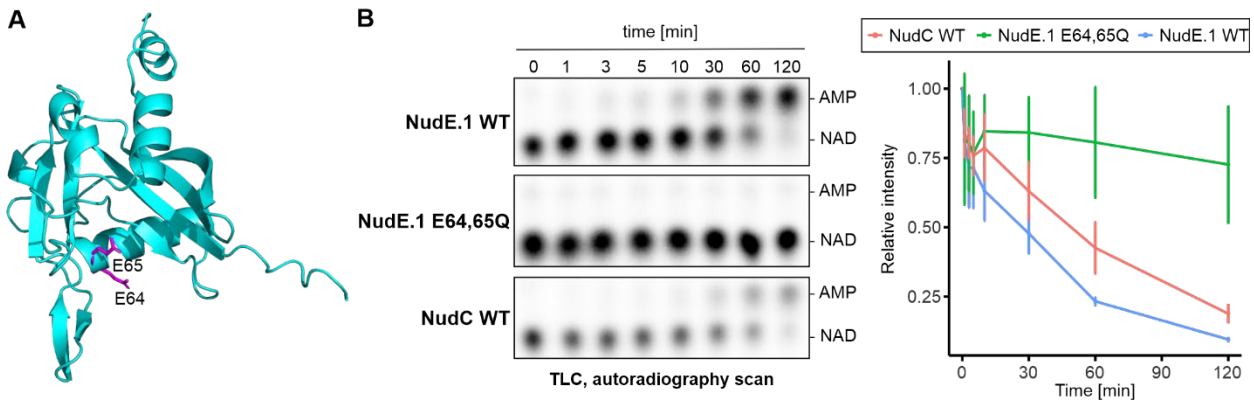

Figure 5: NAD hydrolysis by the T4 phage Nudix hydrolase NudE.1 *in vitro*.
(**A**) Alphafold prediction for NudE.1 indicating E64 and E65 whose mutation to glutamines inactivates NudE.1 (E64,65Q). Prediction metrics are shown in Supplementary Figure S5A. (**B**) Activity of NudE.1 WT, NudE.1 E64,65Q and NudC WT on radiolabeled ^{32}P-NAD *in vitro* as monitored by thin-layer chromatography (TLC) and autoradiography. NudE.1 and NudC WT hydrolyze NAD giving rise to AMP and NMN (n=3).

Next, we set out to test its potential NAD-RNA decapping activity on a 10-nucleotide NAD-RNA with a 3′-Cy5-label (NAD-10mer-Cy5) (Figure 6A). Similar to the known decapping enzyme NudC, NudE.1 efficiently decapped NAD-RNA *in vitro*, whilst the inactive mutant showed no measurable decapping activity (Figure 6B). We then tested whether NudE.1 preferentially decaps distinct RNA structures at the 5′-NAD-cap revealing no clear preference for the structure of the 5′-ends (Figure 6C). The Nudix hydrolase NudC has been reported to act preferentially on NAD-RNA rather than NAD due to its RNA binding affinity. Thus, *in vivo*, where NAD is way more abundant than NAD-RNA (approx. 700-fold molar excess) (6,36,62), NudC hydrolyzes NAD-RNA rather than NAD. To mimic these conditions *in vitro*, we assessed NAD-RNA hydrolysis by NudE.1 and NudC in the absence and the presence of 700- and 1,500-fold molar excess of NAD over NAD-RNA. Notably, increasing NAD levels did not affect decapping by NudC, whilst NAD-cap hydrolysis by NudE.1 was reduced (Figure 6D). However, under physiologically relevant ratios of NAD and NAD-RNA (700:1), NudE.1 still efficiently decapped NAD-RNA *in vitro*. Assessing the levels of NAD over the time course of the kinetic experiments, we barely saw any effects for both NudE.1 and NudC (Supplementary Figure S7D) indicating that both enzymes seem to exert an overall preference for NAD-RNA as substrate *in vitro*. Looking at the structure of NudE.1 in more detail, a positively charged surface is located closely to the negatively charged catalytic site (Supplementary Figure S7B), which may help in recruiting and positioning the NAD-RNA for decapping by NudE.1. This would resemble a mechanistic model similar to the one reported for NudC (24).

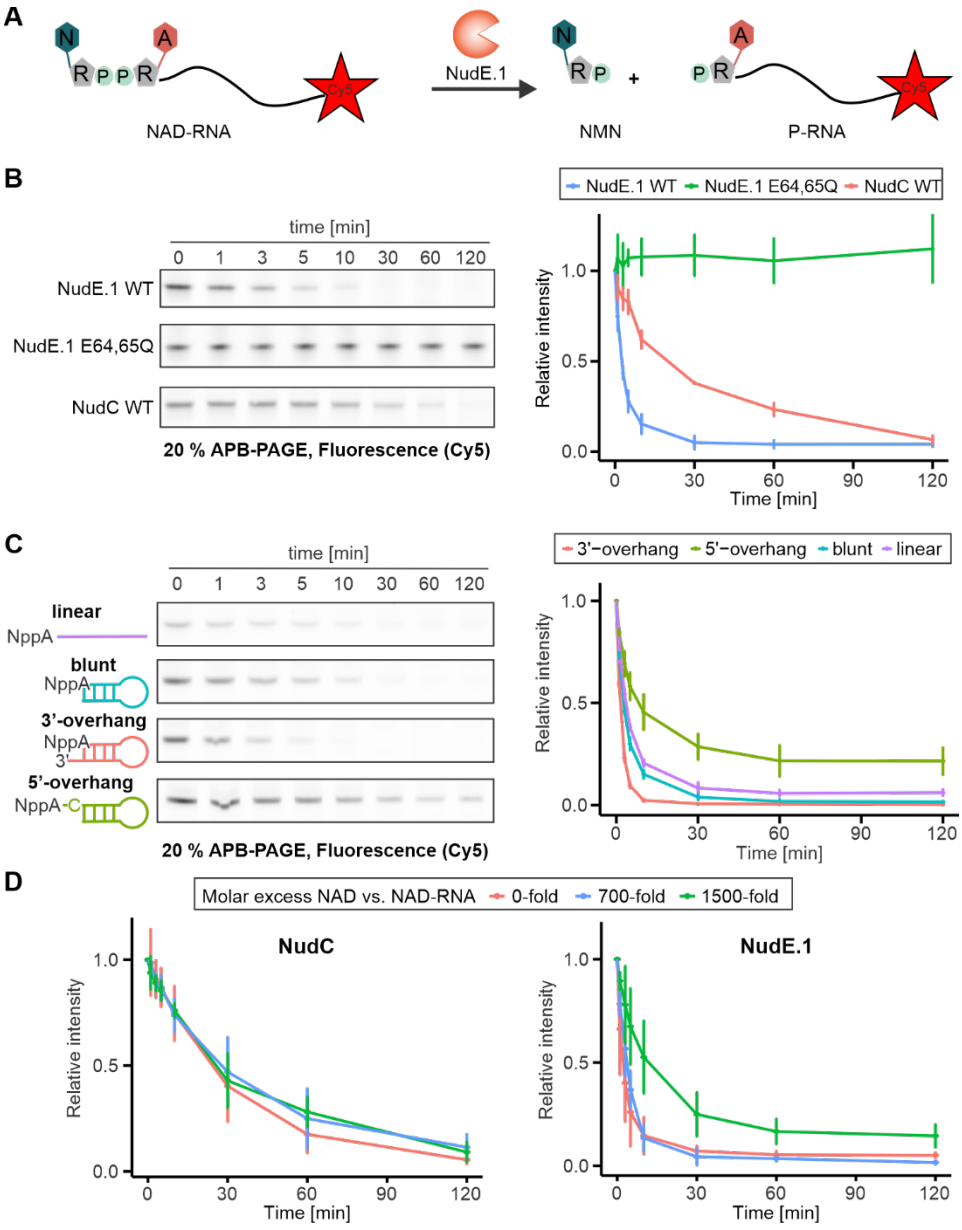

Figure 6: NAD-RNA decapping by the T4 phage Nudix hydrolase NudE.1 *in vitro*.
(**A**) Reaction scheme for the NAD-RNA decapping by NudE.1 by hydrolysis of the pyrophosphate moiety in the NAD-cap. The resulting monophosphorylated RNA is separated from NAD-RNA during APB-PAGE. (**B**) NudE.1 WT efficiently decaps NAD-RNA *in vitro*. Cy5 scan visualizes NAD-RNA and 20 % APB-PAGE is employed to separate NAD- and PPP-RNA thereby indicating the specific decapping activity on NAD-RNA substrate (n=3). (**C**) Decapping activity dependence of NudE.1 on RNA substrate's secondary structure analyzed by 20 % APB-PAGE and fluorescent Cy5 scan (n=3). (**D**) Effects of molar excess of NAD over NAD-RNA on the decapping activity of NudE.1 *in vitro* (n=3). Increasing the molar excess of NAD gradually decreases NudE.1 mediated NAD-RNA decapping (right panel), whilst decapping by NudC was barely affected (left panel).

Influence of NudE.1 on T4 phage infection of *E. coli*

To elucidate the functional role of NudE.1 *in vivo*, during T4 phage infection, we created a T4 phage with catalytically inactive NudE.1 (T4 NudE.1 E64,65Q) and characterized the phenotype of the latter (38). T4 NudE.1 E64,65Q displayed a lysis delayed significantly by approx. 15 minutes compared to T4 WT (Figure 7A,B). Further, we detected similar amount of progeny released by T4 NudE.1 E64,65Q and T4 WT and similar burst sizes of both phages (Figure 7C, Supplementary Table S9). This agrees with previous studies that assessed a NudE.1 deletion T4 phage (37) and described the auxiliary role of *nudE.1* gene during T4 phage infection (32).

To characterize the function of NudE.1 *in vivo* - in the context of infection – we first assessed potential changes of the metabolome of T4 phage infected *E. coli* induced by loss of NudE.1 catalytic activity. Therefore, we compared the endometabolome of T4 WT and T4 NudE.1 E64,65Q infected *E. coli* B strain using LC-MS. The analysis was directed at NAD and two other metabolites that serve as cofactor caps, namely FAD and UDP-N-acetylglucosamine (UDP-GlcNAc) (1), to monitor potential influences of T4 phage infection and NudE.1 on the various cofactor-caps existing in a bacterial cell. We assessed the levels of the three metabolites per *E. coli* cell before (t0) and at two time points post infection (t10, t20). In average, we detected 1.01 x 10^{-4} M FAD, 2.34 x 10^{-3} M NAD and 1.09 x 10^{-3} M UDP-GlcNAc per *E. coli* cell before infection (t0). The measured FAD and NAD concentrations agree well with previously reported metabolite concentrations in *E. coli* (FAD: 1.7 x 10^{-4} M; NAD: 2.6 x 10^{-3} M) (62). UDP-GlcNAc concentrations deviate from previously reported values by approx. 9-fold (UDP-GlcNAc: 9.6 x 10^{-3} M) (62). Upon T4 phage infection the FAD pool did not seem to be affected compared to uninfected *E. coli* (Supplementary Figure S8A). In contrast, we detected a slight increase of UDP-GlcNAc levels over the time course of infection (Supplementary Figure S8B). Interestingly, the NAD pool significantly decreased by almost half upon T4 phage infection (still at approx. 1.5 mM) while remaining constant in uninfected *E. coli* (Figure 7D). In comparison, several phage defense systems employ NAD depletion to abort infection (27-29), which reduce NAD levels by almost half (28) to 5-fold (27,29). Thus, the NAD levels in *E. coli* decrease in a similar manner during T4 phage infection as induced by some phage defense systems. Comparing T4 WT and T4 NudE.1 E64,65Q infection, all three analyzed cofactors displayed similar trends (Figure 7D, Supplementary Figure S8). Consequently, one cannot clearly conclude that NudE.1 specifically modulates cofactors, such as NAD, during T4 phage infection.

In order to investigate a role of NudE.1 in decapping NAD-RNAs during infection, we used LC-MS to determine NAD-cap levels in total RNA from *E. coli* infected with T4 NudE.1 E64,65Q. Upon T4 NudE.1 E64,65Q infection, NAD-cap levels only slightly increased to a median of 0.42 NAD-caps per million nucleotides compared to T4 WT infection (Figure 7E). Consequently, NAD-cap levels are similar in uninfected, T4 WT and T4 NudE.1 E64,65Q infected *E. coli*. This trend in NAD-RNA levels stands in contrast to NAD reduction observed upon infection (Figure 7D), which indicates

that the dynamic NAD-RNA pool is not solely regulated by the available cellular NAD pool. Further, NudE.1 does not appear to exert a specific role in NAD-RNA decapping during T4 phage infection.

In conclusion, our findings indicate NudE.1 as the first phage-derived decapping enzyme *in vitro*. Further, our findings do not suggest a unique role for NudE.1 in regulating the NAD or NAD-RNA pool *in vivo*, but its catalytic function is required for efficient phage infection.

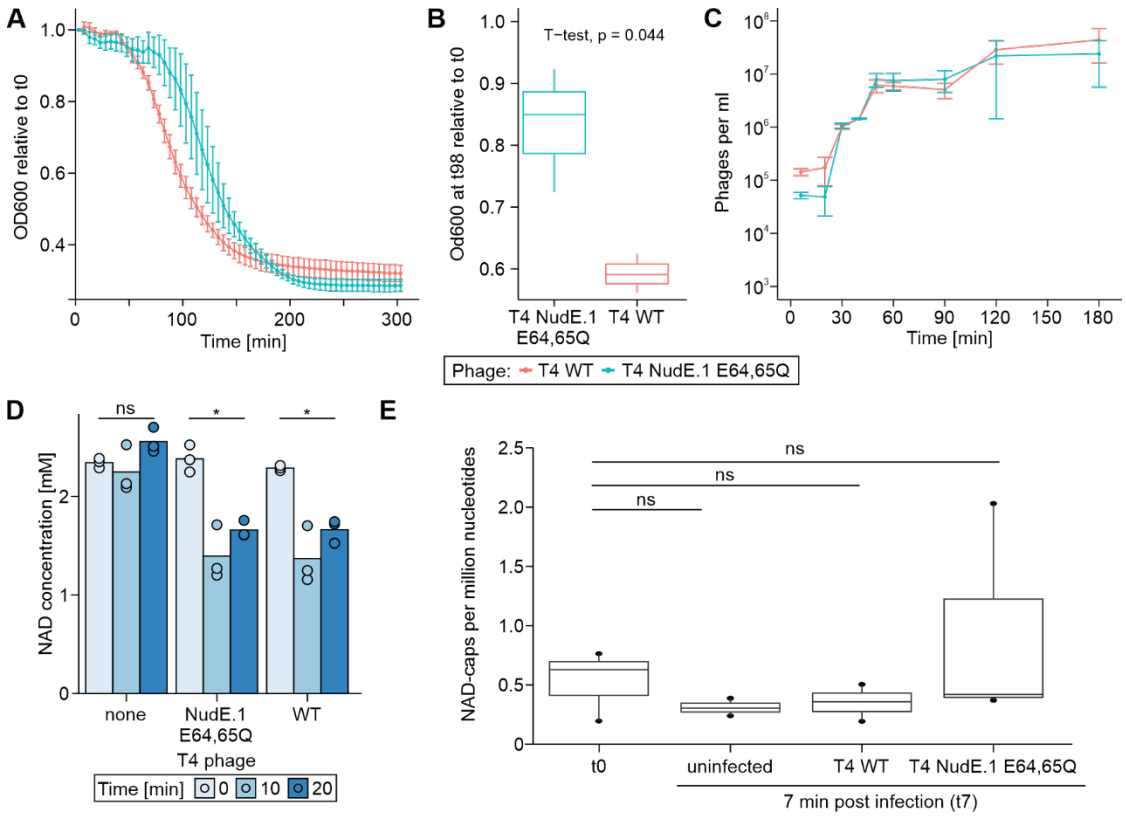

Figure 7: Phenotype of the NudE.1 E64,65Q mutant T4 phage compared to T4 phage WT.
(A) Lysis curves of T4 phage WT and T4 phage NudE.1 E64,65Q (T4 NudE.1 E64,65Q) upon infection of *E. coli* B strain measured as OD_{600} over the time course of infection (n=3). OD_{600} values are normalized relative to the initial measurement at t0. **(B)** T-test comparing OD_{600} of T4 WT and T4 NudE.1 E64,65Q infected *E. coli* B strain at 98 minutes post infection given data presented in A (t-test, two-sided, p = 0.029 at $p_{signif} < 0.05$). **(C)** Progeny released from T4 WT and T4 NudE.1 E64,65Q infected *E. coli* measured as phages per mL over the time course of the burst size assay (n=3). **(D)** Metabolomics analysis of NAD levels in *E. coli* infected with T4 WT, T4 NudE.1 E64,65Q or uninfected (none) over the time course of infection (n=3). NAD concentration [mM] refers to the concentration in an *E. coli* cell of 1 fL volume. **(E)** Same data as presented in Figure 3C complemented by measurements for T4 NudE.1 E64,65Q infection (n=3). We note that the T4 NudE.1 E64,65Q infection sample set likely contains one statistical outlier. NAD concentrations before infection (t0) and 7 min post infection (t7) were compared for each condition using Welch two-sample t-test ($p_{signif} < 0.05$, ns: non-significant).

CONCLUSION AND OUTLOOK

Here, we present the first study that analyses the presence of an RNA modification in the context of a phage-host interaction. We used NAD captureSeq to identify NAD-RNAs over the time course of T4 phage infection of *E. coli*. Our results indicate that the NAD-cap epitranscriptome is dynamically modulated during T4 phage infection (Figure 8). Importantly, we show that both host and phage transcripts possess NAD-caps, which we refer to as the dual NAD-cap epitranscriptome of T4 phage infection.

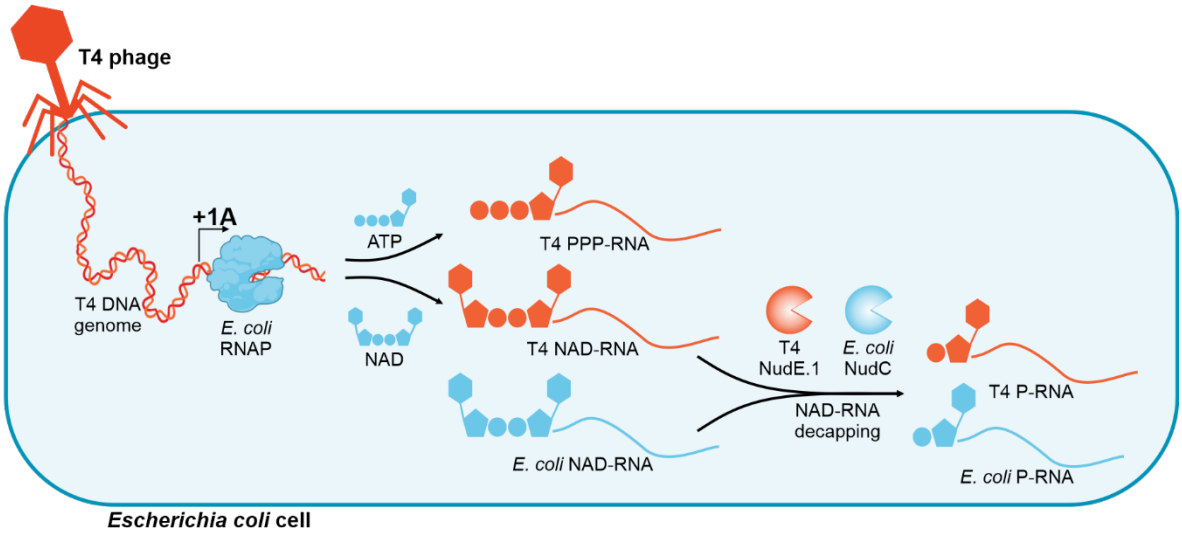

Figure 8: Proposed model for the dynamic NAD-cap epitranscriptome during T4 phage infection. Once the T4 phage injects its DNA genome into the *E. coli* host cell, the host RNAP transcribes T4 phage genes. At +1A TSS, the host RNAP can either canonically initiate transcription resulting in 5'-triphosphorylated RNA (PPP-RNA) or NAD-cap transcripts (NAD-RNA). Both host and T4 NAD-RNAs may be decapped through Nudix hydrolases NudC (host) or NudE.1 (T4 phage). Thereby, NAD-capping through host RNAP and decapping via Nudix hydrolases dynamically modulates the NAD-cap epitranscriptome during T4 phage infection. T4 phage and RNAP elements were created with BioRender.com.

Transcription start site analysis via dRNA-Seq suggests that both phage and host NAD-RNAs during T4 phage infection are indeed synthesized by the *E. coli* RNAP. However, transcription is a complex and tightly regulated process during T4 phage infection and phage infections in general (32,76). It could be an exciting prospect to study how different phage promoters, transcriptional modulators (76) or the post-translational modification of the RNAP (77) may affect the incorporation of RNA modifications such as the NAD-cap in both host and phage transcripts. For instance, T4 phage employs the ADP-ribosyltransferases Alt and ModA to direct the specificity of the host RNAP towards distinct T4 phage genes in the early and middle phase of infection (77,78). Moreover, other phages encode diverse single- and multi-subunit RNA polymerases (79,80), such as T7 RNAP, which perform cofactor-capping of RNAs, such as NAD-capping, with high efficiency

in vitro (81). This suggests that NAD-caps and other RNA modifications may be widespread across different clades of phages infecting different bacterial species (35).

Yet, it remains to be addressed, which purposes the NAD-cap may serve during T4 phage infection. Just recently, the NAD-cap was found to activate RNAs for enzymatic transfer to host proteins by the T4 phage ADP-ribosyltransferase ModB in an RNAylation reaction (36). Both phage and host transcripts were identified as substrates for the RNAylation – specifically being covalently attached to the ribosomal protein S1 during T4 phage infection (36). Here, we are able to validate some of these substrate RNAs from both phage and host by identifying them as NAD-capped, such as phage mRNAs from genes *56*, *59* or *rIII* or host mRNAs derived from *aspA* or *acpP* genes. This further supports the role of NAD-RNAs in RNAylation, as NAD-capping of substrate RNAs is a prerequisite for this reaction (36).

NAD serves as a central regulatory molecule in phage infections and we now show that it caps not only host but also phage RNAs. Many phage defense systems employ NAD depletion as a strategy (27-29) exemplifying that the bacterial host can actively control the NAD pool to counteract phage infection. Thus, it is surprising that T4 phage transcripts are NAD-capped *per se*. We detected that the NAD levels decrease upon T4 phage infection, which could potentially be triggered by a phage defense system such as the Thoeris system (82). Simultaneously, total NAD-RNA levels appeared comparably stable upon T4 phage infection. On this basis, one could speculate that NAD may be more stable, when incorporated into RNA as a cap than its free form. Nevertheless, given the dynamic nature of the NAD-cap epitranscriptome during infection, both host and phage NAD-RNAs may be subject to active RNA decay.

What are the underlying principles of NAD and NAD-RNA regulation during T4 phage infection? NAD-RNA decapping could also involve a host factor, for instance, the host Nudix hydrolase NudC that mediates NAD-RNA decapping *in E. coli* (24). Interestingly, available proteomics data suggest that NudE.1 is up to 60-fold more abundant than *E. coli* NudC during T4 phage infection (34). With NudE.1 the T4 phage could exploit its own factor to regulate the NAD-RNA and NAD pool. Therefore, we characterized the phage Nudix hydrolase NudE.1, which was described to exert activity on various cofactors (37), *in vitro* and *in vivo*. Thereby, we identified NudE.1 to act as an NAD hydrolyzing and NAD-RNA decapping enzyme *in vitro*. This could equip the phage with a means to regulate the NAD and NAD-RNA pools during infection resembling an additional way to fine-tune the takeover and control of the host cell (32,76). Based on the T4 NudE.1 E64,65Q mutant, we did not record an influence of NudE.1 on NAD and NAD-RNA *in vivo*. However, the delayed lysis phenotype of T4 phage with catalytically inactive NudE.1 E64,65Q highlights its assistant function in driving an efficient phage infection. Thus, the role of NudE.1 *in vivo* still needs to be deciphered. Nevertheless, NudE.1 may become a useful molecular biology tool given the activities reported in this and a previous study (37) and exemplifies the rich resource of versatile enzymatic activities that phages provide. The *Vibrio* phage KVP40, for instance, employs a Nudix

hydrolase in a NAD salvage pathway to actively synthesize NAD during infection (83). Given the predicted existence of Nudix hydrolases in other phages (83), this class of enzymes may harbor the potential to target specific metabolites and cofactor-caps to modulate the infection process. For instance, homologues of NudE.1 can be found in various phages targeting *Escherichia*, *Salmonella* and *Shigella* (Supplementary Table S10).

Overall, this study is – to our knowledge – the first to identify viral NAD-RNAs and assess their dynamics during infection. We thereby underline bacteriophage epitranscriptomics as an important field of research. Given that cofactor-capping also plays a role in eukaryotic viruses preventing immune recognition (4), RNA modifications could play yet unidentified roles in (prokaryotic) virus-host interactions such as defense mechanisms in the interplay of phages and bacteria (35).

DATA AVAILABILITY

Custom scripts, analyses and associated data are available under https://github.com/MaikTungsten/PhageEpitranscriptomics. Differential RNA-Seq data is deposited in GEO database under accession GSE255091. Nanopore sequencing data from NAD captureSeq is available from SRA under Bio Project PRJNA1073512. Nanopore data for T4 phage NudE.1 E64,65Q mutant screening is deposited in SRA under Bio Project PRJNA1075486.

SUPPLEMENTARY DATA

Supplementary Data are available at NAR online.

AUTHOR CONTRIBUTIONS

M.W.-S. and A.M. performed total RNA isolations, established and performed NAD captureSeq, performed qPCRs to validate sequencing data. M.W.-S. cloned, expressed, purified and characterized NudE.1. M.W.-S. prepared samples for metabolomics, proteomics and performed experiments to validate NAD-RNAs including Northern blots. N.Po. performed T4 phage mutagenesis and screening PCR, A.A.R.R. performed barcoding and Nanopore sequencing, supervised by D.S. M.W.-S. analysed all sequencing data. M.W.-S. characterized the T4 phage mutant. M.W.-S. prepared samples for LC-MS/MS, N.Pa. performed metabolomics measurements, N.Pa. and M.W-S. analysed the data. S.K. performed quantitative nucleoside MS analysis. K.H. supervised the work. M.W.-S. and K.H. designed the study and wrote the first draft of the manuscript. All other co-authors contributed to editing and proof-reading.

ACKNOWLEDGEMENTS

We thank Peter Claus, Petra Mann and Ahmet Sanal for experimental assistance and the entire team of the Höfer lab and collaborators for fruitful discussions and the nice working environment.

FUNDING

M.W.-S. is supported by funding from the Joachim Herz Foundation (Add-on Fellowships for Interdisciplinary Life Science) and the Studienstiftung des deutschen Volkes e.V. (PhD scholarship). K.H. receives funding from the German Research Council (DFG: SPP 2330 project number 464500427, RTG 2355 project 11 and RTG 2927 project 06), the European Research Council (Belgium) under the European Union's Horizon 2020 research and innovation programme (ERC-2023-STG grant 101114948, NAD-ART) and the Max Planck Society (Max Planck Research Group Leader funding). A.A.R.R and D.S. are supported by the Max Planck Society within the framework of the MaxGENESYS project. S.K. is funded by the European Union through H2020-WIDESPREAD-2020-5 ID-952373 (EpiViral) and the German research Council (DFG: SFB1309: 325871075).

CONFLICT OF INTEREST

K.H. and M.W.-S. filed a European Patent Application (No. 24 157 075.3, NudE.1). The other authors declare no competing interest.

REFERENCES

1. Schauerte, M., Pozhydaieva, N. and Höfer, K. (2021) Shaping the Bacterial Epitranscriptome-5'-Terminal and Internal RNA Modifications. *Adv Biol (Weinh)*, **5**, e2100834.
2. Shi, H., Chai, P., Jia, R. and Fan, X. (2020) Novel insight into the regulatory roles of diverse RNA modifications: Re-defining the bridge between transcription and translation. *Mol Cancer*, **19**, 78.
3. Furuichi, Y. (2015) Discovery of m(7)G-cap in eukaryotic mRNAs. *Proc Jpn Acad Ser B Phys Biol Sci*, **91**, 394-409.
4. Sherwood, A.V., Rivera-Rangel, L.R., Ryberg, L.A., Larsen, H.S., Anker, K.M., Costa, R., Vagbo, C.B., Jakljevic, E., Pham, L.V., Fernandez-Antunez, C. *et al.* (2023) Hepatitis C virus RNA is 5'-capped with flavin adenine dinucleotide. *Nature*, **619**, 811-818.
5. Cahova, H., Winz, M.L., Höfer, K., Nübel, G. and Jäschke, A. (2015) NAD captureSeq indicates NAD as a bacterial cap for a subset of regulatory RNAs. *Nature*, **519**, 374-377.
6. Chen, Y.G., Kowtoniuk, W.E., Agarwal, I., Shen, Y. and Liu, D.R. (2009) LC/MS analysis of cellular RNA reveals NAD-linked RNA. *Nat Chem Biol*, **5**, 879-881.
7. Wang, J., Alvin Chew, B.L., Lai, Y., Dong, H., Xu, L., Balamkundu, S., Cai, W.M., Cui, L., Liu, C.F., Fu, X.Y. *et al.* (2019) Quantifying the RNA cap epitranscriptome reveals novel caps in cellular and viral RNA. *Nucleic Acids Res*, **47**, e130.
8. Wolfram-Schauerte, M. and Höfer, K. (2023) NAD-capped RNAs - a redox cofactor meets RNA. *Trends Biochem Sci*, **48**, 142-155.
9. Hu, H., Flynn, N., Zhang, H., You, C., Hang, R., Wang, X., Zhong, H., Chan, Z., Xia, Y. and Chen, X. (2021) SPAAC-NAD-seq, a sensitive and accurate method to profile NAD(+)-capped transcripts. *P Natl Acad Sci USA*, **118**.
10. Zhang, H., Zhong, H., Wang, X., Zhang, S., Shao, X., Hu, H., Yu, Z., Cai, Z., Chen, X. and Xia, Y. (2021) Use of NAD tagSeq II to identify growth phase-dependent alterations in E. coli RNA NAD(+) capping. *P Natl Acad Sci USA*, **118**.
11. Morales-Filloy, H.G., Zhang, Y., Nübel, G., George, S.E., Korn, N., Wolz, C. and Jäschke, A. (2020) The 5' NAD Cap of RNAIII Modulates Toxin Production in Staphylococcus aureus Isolates. *J Bacteriol*, **202**.
12. Frindert, J., Zhang, Y., Nübel, G., Kahloon, M., Kolmar, L., Hotz-Wagenblatt, A., Burhenne, J., Haefeli, W.E. and Jäschke, A. (2018) Identification, Biosynthesis, and Decapping of NAD-Capped RNAs in B. subtilis. *Cell Rep*, **24**, 1890-1901 e1898.
13. Ruiz-Larrabeiti, O., Benoni, R., Zemlianski, V., Hanišáková, N., Schwarz, M., Brezovská, B., Benoni, B., Hnilicová, J., Kaberdin, V.R., Cahová, H. *et al.* (2021) NAD+ capping of RNA in Archaea and Mycobacteria. *bioRxiv*, 2021.2012.2014.472595.
14. Gomes-Filho, J.V., Breuer, R., Morales-Filloy, H.G., Pozhydaieva, N., Borst, A., Paczia, N., Soppa, J., Hofer, K., Jaschke, A. and Randau, L. (2023) Identification of NAD-RNA species and ADPR-RNA decapping in Archaea. *Nat Commun*, **14**, 7597.
15. Walters, R.W., Matheny, T., Mizoue, L.S., Rao, B.S., Muhlrad, D. and Parker, R. (2017) Identification of NAD+ capped mRNAs in Saccharomyces cerevisiae. *P Natl Acad Sci USA*, **114**, 480-485.

16. Zhang, Y., Kuster, D., Schmidt, T., Kirrmaier, D., Nübel, G., Ibberson, D., Benes, V., Hombauer, H., Knop, M. and Jäschke, A. (2020) Extensive 5'-surveillance guards against non-canonical NAD-caps of nuclear mRNAs in yeast. *Nat Commun*, **11**, 5508.
17. Zhang, H., Zhong, H., Zhang, S., Shao, X., Ni, M., Cai, Z., Chen, X. and Xia, Y. (2019) NAD tagSeq reveals that NAD(+)-capped RNAs are mostly produced from a large number of protein-coding genes in Arabidopsis. *P Natl Acad Sci USA*, **116**, 12072-12077.
18. Dong, H., Wang, X., Tan, C., Gao, L., Cui, J., Liu, L., Mo, B., Xing, Y., Yu, Y. and Chen, X. (2022) NAD(+)-capped RNAs are widespread in rice (Oryza sativa) and spatiotemporally modulated during development. *Sci China Life Sci*, **65**, 2121-2124.
19. Wang, Y., Li, S., Zhao, Y., You, C., Le, B., Gong, Z., Mo, B., Xia, Y. and Chen, X. (2019) NAD(+)-capped RNAs are widespread in the Arabidopsis transcriptome and can probably be translated. *P Natl Acad Sci USA*, **116**, 12094-12102.
20. Niu, K., Zhang, J., Ge, S., Li, D., Sun, K., You, Y., Qiu, J., Wang, K., Wang, X., Liu, R. *et al.* (2023) ONE-seq: epitranscriptome and gene-specific profiling of NAD-capped RNA. *Nucleic Acids Res*, **51**, e12.
21. Jiao, X., Doamekpor, S.K., Bird, J.G., Nickels, B.E., Tong, L., Hart, R.P. and Kiledjian, M. (2017) 5' End Nicotinamide Adenine Dinucleotide Cap in Human Cells Promotes RNA Decay through DXO-Mediated deNADding. *Cell*, **168**, 1015-1027 e1010.
22. Bird, J.G., Zhang, Y., Tian, Y., Panova, N., Barvik, I., Greene, L., Liu, M., Buckley, B., Krasny, L., Lee, J.K. *et al.* (2016) The mechanism of RNA 5' capping with NAD+, NADH and desphospho-CoA. *Nature*, **535**, 444-447.
23. Sharma, S., Yang, J., Grudzien-Nogalska, E., Shivas, J., Kwan, K.Y. and Kiledjian, M. (2022) Xrn1 is a deNADding enzyme modulating mitochondrial NAD-capped RNA. *Nat Commun*, **13**.
24. Höfer, K., Li, S., Abele, F., Frindert, J., Schlotthauer, J., Grawenhoff, J., Du, J., Patel, D.J. and Jäschke, A. (2016) Structure and function of the bacterial decapping enzyme NudC. *Nat Chem Biol*, **12**, 730-734.
25. Westermann, A.J., Forstner, K.U., Amman, F., Barquist, L., Chao, Y., Schulte, L.N., Muller, L., Reinhardt, R., Stadler, P.F. and Vogel, J. (2016) Dual RNA-seq unveils noncoding RNA functions in host-pathogen interactions. *Nature*, **529**, 496-501.
26. Benoni, B., Benoni, R., Trylcova, J., Grab, K., Pačes, J., Weber, J., Stanek, D., Kowalska, J., Bednarova, L., Keckesova, Z. *et al.* (2022) HIV-1 infection reduces NAD capping of host cell snRNA and snoRNA. *bioRxiv*, 2022.2011.2010.515957.
27. Garb, J., Lopatina, A., Bernheim, A., Zaremba, M., Siksnys, V., Melamed, S., Leavitt, A., Millman, A., Amitai, G. and Sorek, R. (2022) Multiple phage resistance systems inhibit infection via SIR2-dependent NAD(+) depletion. *Nat Microbiol*, **7**, 1849-1856.
28. Zaremba, M., Dakineviciene, D., Golovinas, E., Zagorskaite, E., Stankunas, E., Lopatina, A., Sorek, R., Manakova, E., Ruksenaite, A., Silanskas, A. *et al.* (2022) Short prokaryotic Argonautes provide defence against incoming mobile genetic elements through NAD(+) depletion. *Nat Microbiol*, **7**, 1857-1869.
29. Ofir, G., Herbst, E., Baroz, M., Cohen, D., Millman, A., Doron, S., Tal, N., Malheiro, D.B.A., Malitsky, S., Amitai, G. *et al.* (2021) Antiviral activity of bacterial TIR domains via immune signalling molecules. *Nature*, **600**, 116-120.

30. Osterman, I., Samra, H., Rousset, F., Loseva, E., Itkin, M., Malitsky, S., Yirmiya, E., Millman, A. and Sorek, R. (2024) Phages reconstitute NAD⁺ to counter bacterial immunity. *bioRxiv*, 2024.2002.2011.579819.
31. Chen, T.H., Potapov, V., Dai, N., Ong, J.L. and Roy, B. (2022) N(1)-methyl-pseudouridine is incorporated with higher fidelity than pseudouridine in synthetic RNAs. *Sci Rep*, **12**, 13017.
32. Miller, E.S., Kutter, E., Mosig, G., Arisaka, F., Kunisawa, T. and Rüger, W. (2003) Bacteriophage T4 genome. *Microbiol Mol Biol Rev*, **67**, 86-156, table of contents.
33. Luke, K., Radek, A., Liu, X., Campbell, J., Uzan, M., Haselkorn, R. and Kogan, Y. (2002) Microarray analysis of gene expression during bacteriophage T4 infection. *Virology*, **299**, 182-191.
34. Wolfram-Schauerte, M., Pozhydaieva, N., Viering, M., Glatter, T. and Höfer, K. (2022) Integrated Omics Reveal Time-Resolved Insights into T4 Phage Infection of E. coli on Proteome and Transcriptome Levels. *Viruses-Basel*, **14**, 2502.
35. Pozhydaieva, N., Wolfram-Schauerte, M., Keuthen, H. and Höfer, K. (2024) The enigmatic epitranscriptome of bacteriophages: putative RNA modifications in viral infections. *Curr Opin Microbiol*, **77**, 102417.
36. Wolfram-Schauerte, M., Pozhydaieva, N., Grawenhoff, J., Welp, L.M., Silbern, I., Wulf, A., Billau, F.A., Glatter, T., Urlaub, H., Jäschke, A. *et al.* (2023) A viral ADP-ribosyltransferase attaches RNA chains to host proteins. *Nature*, **620**, 1054-1062.
37. Xu, W., Gauss, P., Shen, J., Dunn, C.A. and Bessman, M.J. (2002) The gene e.1 (nudE.1) of T4 bacteriophage designates a new member of the Nudix hydrolase superfamily active on flavin adenine dinucleotide, adenosine 5'-triphospho-5'-adenosine, and ADP-ribose. *J Biol Chem*, **277**, 23181-23185.
38. Pozhydaieva, N., Billau, F.A., Wolfram-Schauerte, M., Rojas, A.A.R., Paczia, N., Schindler, D. and Höfer, K. (2024) Temporal epigenome modulation enables efficient bacteriophage engineering and functional analysis of phage DNA modifications. *bioRxiv*, 2024.2001.2028.577628.
39. Ramirez Rojas, A.A., Brinkmann, C.K., Kobel, T.S. and Schindler, D. (2024) DuBA.flow horizontal line A Low-Cost, Long-Read Amplicon Sequencing Workflow for the Validation of Synthetic DNA Constructs. *ACS Synth Biol*.
40. Oberacker, P., Stepper, P., Bond, D.M., Hohn, S., Focken, J., Meyer, V., Schelle, L., Sugrue, V.J., Jeunen, G.J., Moser, T. *et al.* (2019) Bio-On-Magnetic-Beads (BOMB): Open platform for high-throughput nucleic acid extraction and manipulation. *PLoS Biol*, **17**, e3000107.
41. Krehenwinkel, H., Pomerantz, A., Henderson, J.B., Kennedy, S.R., Lim, J.Y., Swamy, V., Shoobridge, J.D., Graham, N., Patel, N.H., Gillespie, R.G. *et al.* (2019) Nanopore sequencing of long ribosomal DNA amplicons enables portable and simple biodiversity assessments with high phylogenetic resolution across broad taxonomic scale. *Gigascience*, **8**.
42. Li, H. (2018) Minimap2: pairwise alignment for nucleotide sequences. *Bioinformatics*, **34**, 3094-3100.
43. Danecek, P., Bonfield, J.K., Liddle, J., Marshall, J., Ohan, V., Pollard, M.O., Whitwham, A., Keane, T., McCarthy, S.A., Davies, R.M. *et al.* (2021) Twelve years of SAMtools and BCFtools. *Gigascience*, **10**.
44. Edge, P. and Bansal, V. (2019) Longshot enables accurate variant calling in diploid genomes from single-molecule long read sequencing. *Nat Commun*, **10**, 4660.

45. Thorvaldsdottir, H., Robinson, J.T. and Mesirov, J.P. (2013) Integrative Genomics Viewer (IGV): high-performance genomics data visualization and exploration. *Brief Bioinform*, **14**, 178-192.
46. Nübel, G., Sorgenfrei, F.A. and Jäschke, A. (2017) Boronate affinity electrophoresis for the purification and analysis of cofactor-modified RNAs. *Methods*, **117**, 14-20.
47. Winz, M.L., Cahova, H., Nübel, G., Frindert, J., Höfer, K. and Jäschke, A. (2017) Capture and sequencing of NAD-capped RNA sequences with NAD captureSeq. *Nat Protoc*, **12**, 122-149.
48. Leger, A. and Leonardi, T. (2019) pycoQC, interactive quality control for Oxford Nanopore Sequencing. *Journal of Open Source Software*, **4**, 1236.
49. Liao, Y., Smyth, G.K. and Shi, W. (2014) featureCounts: an efficient general purpose program for assigning sequence reads to genomic features. *Bioinformatics*, **30**, 923-930.
50. Thomason, M.K., Bischler, T., Eisenbart, S.K., Förstner, K.U., Zhang, A., Herbig, A., Nieselt, K., Sharma, C.M. and Storz, G. (2015) Global transcriptional start site mapping using differential RNA sequencing reveals novel antisense RNAs in Escherichia coli. *J Bacteriol*, **197**, 18-28.
51. Bailey, T.L., Johnson, J., Grant, C.E. and Noble, W.S. (2015) The MEME Suite. *Nucleic Acids Res*, **43**, W39-49.
52. Förstner, K.U., Vogel, J. and Sharma, C.M. (2014) READemption-a tool for the computational analysis of deep-sequencing-based transcriptome data. *Bioinformatics*, **30**, 3421-3423.
53. Yu, S.H., Vogel, J. and Förstner, K.U. (2018) ANNOgesic: a Swiss army knife for the RNA-seq based annotation of bacterial/archaeal genomes. *Gigascience*, **7**.
54. Dugar, G., Herbig, A., Förstner, K.U., Heidrich, N., Reinhardt, R., Nieselt, K. and Sharma, C.M. (2013) High-resolution transcriptome maps reveal strain-specific regulatory features of multiple Campylobacter jejuni isolates. *Plos Genet*, **9**, e1003495.
55. Höfer, K., Abele, F., Schlotthauer, J. and Jäschke, A. (2016) Synthesis of 5'-NAD-Capped RNA. *Bioconjugate Chem*, **27**, 874-877.
56. Mirdita, M., Schütze, K., Moriwaki, Y., Heo, L., Ovchinnikov, S. and Steinegger, M. (2022) ColabFold: making protein folding accessible to all. *Nat Methods*, **19**, 679-682.
57. Kubitschek, H.E. (1990) Cell volume increase in Escherichia coli after shifts to richer media. *J Bacteriol*, **172**, 94-101.
58. Volkmer, B. and Heinemann, M. (2011) Condition-dependent cell volume and concentration of Escherichia coli to facilitate data conversion for systems biology modeling. *PLoS One*, **6**, e23126.
59. Kellner, S., Neumann, J., Rosenkranz, D., Lebedeva, S., Ketting, R.F., Zischler, H., Schneider, D. and Helm, M. (2014) Profiling of RNA modifications by multiplexed stable isotope labelling. *Chem Commun (Camb)*, **50**, 3516-3518.
60. Sharma, S., Yang, J., Favate, J., Shah, P. and Kiledjian, M. (2023) NADcapPro and circNC: methods for accurate profiling of NAD and non-canonical RNA caps in eukaryotes. *Commun Biol*, **6**, 406.
61. Nabergoj, D., Modic, P. and Podgornik, A. (2018) Effect of bacterial growth rate on bacteriophage population growth rate. *Microbiologyopen*, **7**, e00558.

62. Bennett, B.D., Kimball, E.H., Gao, M., Osterhout, R., Van Dien, S.J. and Rabinowitz, J.D. (2009) Absolute metabolite concentrations and implied enzyme active site occupancy in Escherichia coli. *Nat Chem Biol*, **5**, 593-599.
63. Dai, X., Zhu, M., Warren, M., Balakrishnan, R., Patsalo, V., Okano, H., Williamson, J.R., Fredrick, K., Wang, Y.P. and Hwa, T. (2016) Reduction of translating ribosomes enables Escherichia coli to maintain elongation rates during slow growth. *Nat Microbiol*, **2**, 16231.
64. Shepherd, J. and Ibba, M. (2015) Bacterial transfer RNAs. *Fems Microbiol Rev*, **39**, 280-300.
65. Urbanowski, M.L., Stauffer, L.T. and Stauffer, G.V. (2000) The gcvB gene encodes a small untranslated RNA involved in expression of the dipeptide and oligopeptide transport systems in Escherichia coli. *Mol Microbiol*, **37**, 856-868.
66. Rawlings, M. and Cronan, J.E. (1992) The Gene Encoding Escherichia-Coli Acyl Carrier Protein Lies within a Cluster of Fatty-Acid Biosynthetic Genes. *Journal of Biological Chemistry*, **267**, 5751-5754.
67. Carlioz, A. and Touati, D. (1986) Isolation of superoxide dismutase mutants in Escherichia coli: is superoxide dismutase necessary for aerobic life? *EMBO J*, **5**, 623-630.
68. Hobbs, E.C., Astarita, J.L. and Storz, G. (2010) Small RNAs and small proteins involved in resistance to cell envelope stress and acid shock in Escherichia coli: analysis of a bar-coded mutant collection. *J Bacteriol*, **192**, 59-67.
69. Qi, D., Alawneh, A.M., Yonesaki, T. and Otsuka, Y. (2015) Rapid Degradation of Host mRNAs by Stimulation of RNase E Activity by Srd of Bacteriophage T4. *Genetics*, **201**, 977-987.
70. Munro, J.L. and Wiberg, J.S. (1968) Evidence That Gene 56 of Bacteriophage T4 Is a Structural Gene for Deoxycytidine Triphosphatase. *Virology*, **36**, 442-&.
71. Reichenbach, B., Maes, A., Kalamorz, F., Hajnsdorf, E. and Gorke, B. (2008) The small RNA GlmY acts upstream of the sRNA GlmZ in the activation of glmS expression and is subject to regulation by polyadenylation in Escherichia coli. *Nucleic Acids Res*, **36**, 2570-2580.
72. Sharma, C.M., Hoffmann, S., Darfeuille, F., Reignier, J., Findeiss, S., Sittka, A., Chabas, S., Reiche, K., Hackermuller, J., Reinhardt, R. *et al.* (2010) The primary transcriptome of the major human pathogen Helicobacter pylori. *Nature*, **464**, 250-255.
73. Sharma, C.M. and Vogel, J. (2014) Differential RNA-seq: the approach behind and the biological insight gained. *Curr Opin Microbiol*, **19**, 97-105.
74. Wicke, L., Ponath, F., Coppens, L., Gerovac, M., Lavigne, R. and Vogel, J. (2021) Introducing differential RNA-seq mapping to track the early infection phase for Pseudomonas phage ϕKZ. *Rna Biol*, **18**, 1099-1110.
75. Sutherland, C. and Murakami, K.S. (2018) An Introduction to the Structure and Function of the Catalytic Core Enzyme of Escherichia coli RNA Polymerase. *EcoSal Plus*, **8**.
76. Tabib-Salazar, A., Mulvenna, N., Severinov, K., Matthews, S.J. and Wigneshweraraj, S. (2019) Xenogeneic Regulation of the Bacterial Transcription Machinery. *J Mol Biol*, **431**, 4078-4092.
77. Koch, T., Raudonikiene, A., Wilkens, K. and Rüger, W. (1995) Overexpression, purification, and characterization of the ADP-ribosyltransferase (gpAlt) of bacteriophage T4: ADP-ribosylation of E. coli RNA polymerase modulates T4 "early" transcription. *Gene Expr*, **4**, 253-264.

78. Tiemann, B., Depping, R. and Rüger, W. (1999) Overexpression, purification, and partial characterization of ADP-ribosyltransferases modA and modB of bacteriophage T4. *Gene Expr*, **8**, 187-196.
79. Sokolova, M.L., Misovetc, I. and K, V.S. (2020) Multisubunit RNA Polymerases of Jumbo Bacteriophages. *Viruses*, **12**.
80. Basu, R.S. and Murakami, K.S. (2014) Bacteriophage RNA Polymerases. *Nucleic Acids Mol Bi*, **30**, 237-250.
81. Huang, F. (2003) Efficient incorporation of CoA, NAD and FAD into RNA by in vitro transcription. *Nucleic Acids Res*, **31**, e8.
82. Ka, D., Oh, H., Park, E., Kim, J.H. and Bae, E. (2020) Structural and functional evidence of bacterial antiphage protection by Thoeris defense system via NAD(+) degradation. *Nat Commun*, **11**, 2816.
83. Lee, J.Y., Li, Z. and Miller, E.S. (2017) Vibrio Phage KVP40 Encodes a Functional NAD(+) Salvage Pathway. *J Bacteriol*, **199**.